



2013-06-12

# Simulation of 810 nm Light Propagation Through the Human Finger for Non-Invasive Blood Analysis

Nichole Millward Maughan  
*Brigham Young University - Provo*

Follow this and additional works at: <https://scholarsarchive.byu.edu/etd>

 Part of the [Astrophysics and Astronomy Commons](#), and the [Physics Commons](#)

---

## BYU ScholarsArchive Citation

Maughan, Nichole Millward, "Simulation of 810 nm Light Propagation Through the Human Finger for Non-Invasive Blood Analysis" (2013). *All Theses and Dissertations*. 3707.  
<https://scholarsarchive.byu.edu/etd/3707>

This Thesis is brought to you for free and open access by BYU ScholarsArchive. It has been accepted for inclusion in All Theses and Dissertations by an authorized administrator of BYU ScholarsArchive. For more information, please contact [scholarsarchive@byu.edu](mailto:scholarsarchive@byu.edu), [ellen\\_amatangelo@byu.edu](mailto:ellen_amatangelo@byu.edu).

Simulation of 810 nm Light Propagation Through the Human Finger  
for Non-Invasive Blood Analysis

Nichole M. Maughan

A thesis submitted to the faculty of  
Brigham Young University  
in partial fulfillment of the requirements for the degree of  
Master of Science

J. Ward Moody, Chair  
R. Steven Turley  
David Busath

Department of Physics and Astronomy  
Brigham Young University

June 2013

Copyright © 2013 Nichole M. Maughan

All Rights Reserved

## ABSTRACT

### Simulation of 810 nm Light Propagation Through the Human Finger for Non-Invasive Blood Analysis

Nichole M. Maughan

Department of Physics and Astronomy, BYU  
Master of Science

Non-invasive blood analysis devices that can measure characteristics less prominent than the oxygenation of hemoglobin are of interest in the medical community. An important step in creating these devices is to model the interaction of photons with human tissue in increasingly greater physiological detail. We have modeled, using a Monte Carlo technique, the interaction of photons through epidermis, blood and water arranged both in layers and in a homogeneous mixture. We confirm the expected linear relation between photon attenuation and material volumetric percentage in our two-layer models. We discovered that this relationship becomes non-linear in the homogeneously mixed models where volumetric percentage must be replaced with interaction volume percentage. These nonlinearities become significant when the values of the interaction coefficient,  $\mu_t$ , differ by an order of magnitude or more and could prove crucial in accurately reading oxygenation or other constituents in the blood and also in modeling radiation delivered to a patient in photodynamic therapy.

Keywords: Monte Carlo modeling, light propagation, human tissue, layered, homogeneous mix, non-invasive

## ACKNOWLEDGMENTS

I would like to thank Convergence Biometrics for funding this research, Dr. J. Moody for advising me with this thesis, and David Miller for making this project possible. I would also like to thank my committee members, Dr. Busath and Dr. Turley, for all of the insight they offered on this thesis.

# Contents

<b>Table of Contents</b>	<b>iv</b>
<b>List of Figures</b>	<b>v</b>
<b>1 Introduction</b>	<b>1</b>
1.1 Background . . . . .	1
1.2 Monte Carlo Simulation Method for Light Propagation . . . . .	3
1.3 Modified Beer's Law . . . . .	9
<b>2 Methods and Procedures</b>	<b>11</b>
2.1 Development of Monte Carlo Simulation for Semi-Infinite Pure Tissue Model and Comparison to Previously Published Results . . . . .	12
2.2 Development of Monte Carlo Simulation for Semi-Infinite Layered Tissue Model and Comparison to Previously Published Results . . . . .	18
2.3 Development of Monte Carlo Simulation for Semi-Infinite Homogeneous Mixed Tissue Model . . . . .	27
<b>3 Results and Conclusions</b>	<b>31</b>
<b>A Instructions for using Mathematica</b>	<b>37</b>
<b>B Instructions for using "Monte Carlo Simulation of Photon Propagation" with the layered model</b>	<b>42</b>
<b>C Instructions for using "Monte Carlo Simulation of Photon Propagation" with the mixed model</b>	<b>48</b>
<b>Bibliography</b>	<b>51</b>

# List of Tables

2.1	Absorption ( $\mu_a$ ), scattering ( $\mu_s$ ), transmission ( $\mu_t$ ), and bulk attenuation ( $\alpha$ ) coefficients and anisotropy factor ( $g$ ) of epidermis [11], water [13], and whole blood (Hct=0.45-0.46, oxygenation>98%) [11] at a wavelength of 810 nm. The values for $\alpha_{normalized}$ are the values calculated using Eq. (1.21), normalized by dividing out the $\sqrt{3}$ . The values for $\alpha_{derived}$ are the attenuation coefficients we obtained from fitting an exponential decay to the results from the simulations (see Fig. 2.3). Comparing $\alpha_{normalized}$ to $\alpha_{derived}$ , we see that the two values agree quite well. . . .	12
2.2	Indices of refraction of epidermis [14], water [15], and whole blood [16]. . . . .	19

# List of Figures

1.1	Coordinate System for Scattering Angle . . . . .	6
2.1	Paths are traced of 10 photon packets in Monte Carlo simulation for a semi-infinite slab of blood. The source is at the top, centered at the origin, while the detector is at the bottom, centered at (0,0,1 mm). . . . .	13
2.2	Paths are traced of 10 photon packets in Monte Carlo simulation for a semi-infinite slab of epidermis. The source is at the top, centered at the origin, while the detector is at the bottom, centered at (0,0,1 mm). . . . .	14
2.3	Results of the Monte Carlo simulation for a semi-infinite slab of whole blood, represented by solid blue points. Error bars from Poisson statistics are smaller than most data symbols. The modeled attenuation coefficient $\alpha_{derived}$ is derived from the solid black curve, and substituting the theoretical normalized value, $\alpha_{normalized}$ , into modified Beer's law, Eq. (1.20) gives the dashed red line. One can see that the derived exponential decay curve of the data (solid black) is in good agreement with the modified form of Beer's Law and Eq.(1.21) (dashed red). . . . .	15

2.4 Results of the Monte Carlo simulation for a semi-infinite slab of water, represented by solid blue points. Error bars from Poisson statistics are shown. The modeled attenuation coefficient  $\alpha_{derived}$  is derived from the solid black curve, and substituting the theoretical normalized value,  $\alpha_{normalized}$ , into modified Beer’s law, Eq. (1.20) gives the dashed red line. One can see that the derived exponential decay curve of the data (solid black) is in good agreement with the modified form of Beer’s Law and Eq.(1.21) (dashed red). . . . . 16

2.5 Results of the Monte Carlo simulation for a semi-infinite slab of epidermis, represented by solid blue points. Error bars from Poisson statistics are smaller than most data symbols. The modeled attenuation coefficient  $\alpha_{derived}$  is derived from the solid black curve, and substituting the theoretical normalized value,  $\alpha_{normalized}$ , into modified Beer’s law, Eq. (1.20) gives the dashed red line. One can see that the derived exponential decay curve of the data (solid black) is in good agreement with the modified form of Beer’s Law and Eq.(1.21) (dashed red). . . . . 17

2.6 Semi-infinite layered model for two tissue layers . . . . . 19

2.7 Paths are traced of 10 photon packets in Monte Carlo simulation for a semi-infinite layered slab of 1/2 epidermis (top layer) and 1/2 blood (bottom layer). The source is at the top, centered at the origin, while the detector is at the bottom, centered at (0,0,1 mm). . . . . 23



- 2.8 Bulk attenuation coefficient  $\alpha$  as a function of volume fraction of water in a layered model of water as the layer near the source and blood as the layer near the detector. Statistical error bars are shown for each point, but are too small to see for most points. The coefficient of determination,  $R^2$ , is the statistical value that represents how close the data points follow the linear relationship between  $\alpha$  and the volume fraction of water (dashed line). The results for this model yield  $R^2 = 1.0 \pm 10^{-4}$ . A value of  $R^2 = 1$  represents a perfect correlation. . . . . 24
- 2.9 Bulk attenuation coefficient  $\alpha$  as a function of volume fraction of blood in a layered model of blood then water. Statistical error bars are shown for each point and are large for this model due to noise from reflection at the blood-water interface. The coefficient of determination,  $R^2$ , is the statistical value that represents how close the data points follow the linear relationship between  $\alpha$  and the volume fraction of blood (dashed line). The results for this model yield  $R^2 = 0.849$ . A value of  $R^2 = 1$  represents a perfect correlation. . . . . 25
- 2.10 Bulk attenuation coefficient  $\alpha$  as a function of volume fraction of epidermis in a layered model of epidermis, then blood. Statistical error bars are shown for each point, but are too small to see for many points. The coefficient of determination,  $R^2$ , is the statistical value that represents how close the data points follow the linear relationship between  $\alpha$  and the volume fraction of epidermis (dashed line). The results for this model yield  $R^2 = 1.0 \pm 10^{-4}$ . A value of  $R^2 = 1$  represents a perfect correlation. . . . . 26

2.11 Bulk attenuation coefficient  $\alpha$  as a function of volume fraction of blood in a layered model of blood then epidermis. Statistical error bars are shown for each point. The coefficient of determination,  $R^2$ , is the statistical value that represents how close the data points follow the linear relationship between  $\alpha$  and the volume fraction of water (dashed line). The results for this model yield  $R^2 = 0.999$ . A value of  $R^2 = 1$  represents a perfect correlation. . . . . 27

3.1 Paths are traced of 10 photon packets in Monte Carlo simulation for a semi-infinite slab of a homogeneous mix of 50% epidermis and 50% blood. The source is at the top, centered at the origin, while the detector is at the bottom, centered at (0,0,1 mm). . . . . 32

3.2 Paths are traced of 10 photon packets in Monte Carlo simulation for a semi-infinite slab of a homogeneous mix of 50% water and 50% blood. The source is at the top, centered at the origin, while the detector is at the bottom, centered at (0,0,1 mm). . . . . 32

3.3 Bulk attenuation coefficient  $\alpha$  as a function of volume fraction of water in a mixed model of water and blood. Error bars from Poisson statistics are smaller than most data symbols. The coefficient of determination,  $R^2$ , is 0.889 and represents the value of a linear relationship between  $\alpha$  and the volume fraction of water (red, dashed line) if one existed. . . . . 33

3.4 Bulk attenuation coefficient  $\alpha$  as a function of volume fraction of epidermis in a mixed model of epidermis and blood. Error bars from Poisson statistics are smaller than most data symbols. Statistical error bars are shown for each point, but are too small to see for most points. The coefficient of determination,  $R^2$ , is 0.997 and represents the value of a linear relationship between  $\alpha$  and the volume fraction of blood (red, dashed line) if one existed. . . . . 34

A.1	An example of Mathematica running . . . . .	38
A.2	Quit the Kernel or abort the evaluation . . . . .	39
A.3	Locate the Documentation Center . . . . .	40
A.4	Documentation Center . . . . .	41
B.1	In order to use epidermis and dermis in the same simulation at a specific wavelength, they must both have the coefficients for that specific wavelength. . . . .	43
B.2	Starting the Monte Carlo layered model simulation . . . . .	45
B.3	While the Monte Carlo simulation is running, a number will display at the end of the main code, such as 1000 in the above figure. This number represents the total thickness (in $\mu\text{m}$ ) of the model that the simulation is running through at that moment. This number will change from the value that "min" is set to all the way to the value that "max" is set to in increments of "spacing". One can evaluate the next cell down after the simulation is done to show the paths that the photon packets take in the last thickness the simulation ran through. . . . .	46
B.4	Attenuation Coefficient notebook output for curve-fit to data from Monte Carlo simulation . . . . .	47

# Chapter 1

## Introduction

### 1.1 Background

Pulse oximeters are non-invasive devices that measure the oxygenation of a person's hemoglobin. They are usually placed on a person's fingertip or earlobe [1]. A typical pulse oximeter consists of two small light-emitting diodes (LEDs) that emit light in two different wavelength ranges, visible red and infrared. Oxyhemoglobin absorbs light at these wavelengths differently than the deoxyhemoglobin; thus, the ratio of absorbance oxy/deoxyhemoglobin can be detected and calculated [2]. Furthermore, a user's pulse can be detected simultaneously. Pulse oximeters, first developed in 1972, are now a common device in countless environments including hospitals, work places, airplanes, and even in some homes [3].

Some have extended the techniques of near-infrared spectroscopy (NIRS) used in pulse-oximetry to clinical applications where the focus is shifted from monitoring the overall pulse and blood-oxygen content to monitoring oxygen saturation in specific regions of the patient's body. For example, Murkin et al. [4] discuss the usefulness of cerebral oximetry monitoring where NIRS is used to monitor the oxygen saturation in the cerebral cortex of the brain. Use of these devices during

cardiac surgery allows early detection of cerebral ischaemia (poor blood flow to the brain) before significant damage, such as stroke, occurs. Another example is the use of NIRS in studying the oxygenation in muscle and other tissues for sport sciences. It is a much more practical method for measuring oxygen saturation than other non-invasive techniques such as magnetic resonance spectroscopy since it is much less expensive and it allows for measurements while a subject is moving [5]. Berger et al. developed techniques with NIR Raman spectroscopy to measure analytes in blood and serum such as cholesterol, urea, and total protein [6].

Another application that we are striving towards is creating a non-invasive blood analysis device that can read smaller blood constituents, such as glucose. Such a device would be greatly beneficial to the diabetic community as both type 1 and type 2 diabetics benefit from monitored and controlled levels of glucose. Diabetes is a major cause of heart disease and stroke and is the seventh leading cause of death in the United States. The Center for Disease Control and Prevention (CDC) reports that 8.3% of the U.S. population has diabetes [7]. The people who do not monitor and control their glucose levels properly are at greater risk of countless health complications such as heart disease, stroke, hypertension, blindness, kidney disease, nervous system disease, amputations, etc. [7]. Many people do not monitor their glucose levels as much as they should because of the discomfort and inconvenience associated with a finger prick. If there was a device that did not require needles or pricking of any kind to test blood-glucose levels, more and more diabetics would be willing to monitor their glucose/insulin levels, and in turn there would be fewer diabetes-related incidents and fatalities. Creating an accurate model of the interaction of light with the human finger is an important step towards developing such a non-invasive method for reading novel blood constituent levels.

## 1.2 Monte Carlo Simulation Method for Light Propagation

Monte Carlo simulations can be used to model photon interactions with matter. This method has been used for years in a variety of fields of study and has found particular utility in biomedical optics [8–10]. It requires significant computational resources but is an effective method for starting simple and building to greater complexity as needed [9].

In this Monte Carlo model, photon packets are traced one at a time as they propagate through the media. These packets interact with the molecules of each substance in accordance with their absorptive and scattering properties. Simple absorption follows an exponential relation known as Beer's law. To account for scattering as well requires the use of a modified form of Beer's law (see section 1.3). A modified form of Beer's law is needed because light propagation within a tissue sample is dominated by scattering (the scattering coefficients are two orders of magnitude larger than the absorption coefficients) [8]. The scattering of light within each material depends on all of its constituents: cells (0.1 nm-100 nm), cell organelles (10 nm-10  $\mu$ m), and fiber structures (10-400 nm in diameter) [11].

The method begins with launching a packet of photons into the medium with a photon "weight" equal to one. This weight represents the total incident intensity of the photon packet and diminishes at each event or interaction within the various media [8]. A packet is completely absorbed and its weight or overall intensity becomes negligible when all of the photons in that packet are terminated [8]. In our simulations, we set the emitter with a diameter of 1 mm centered about the origin and launch the photon packets in the  $-z$ -direction, normal to the interface. Photon packets are launched from any point within the defined emitter region. We take a random number,  $\beta$ , between 0 and 1, and let the initial location of the photon packet be

$$x = r \cos(2\pi\beta) \quad (1.1)$$

$$y = r \sin(2\pi\beta) \quad (1.2)$$

$$z = 0 \quad (1.3)$$

where  $r$  is the radius of the emitter. The detector with a diameter of 1 mm is placed at a location  $(0, 0, -bb)$ , where  $bb > 0$ . When a photon packet hits the detector, its remaining intensity is recorded, and a new photon packet is launched. The sizes of the emitter and detector are chosen to be 1 mm because this is a fairly standard size in the industry. We understand that changing the size of the detector could effect the results of the simulation as it could skew how the material appears to scatter the photon packets, but because we are using LEDs and detectors with a size of 1 mm in diameter in our clinical trials, we use this size in our simulations.

Photon packets travel a "propagation distance" between interactions. This distance is based on the transmission coefficient, also known as the interaction coefficient, of the material that makes up the medium. The transmission coefficient,  $\mu_t$ , is the probability of a photon interaction per unit pathlength [8]. We can write  $\mu_t$  in terms of the absorption ( $\mu_a$ ) and scattering ( $\mu_s$ ) coefficients, which are the probabilities of photon absorption and scattering per unit path length, respectively, and have units of  $\text{mm}^{-1}$  [8, 10]:

$$\mu_t = \mu_a + \mu_s \quad (1.4)$$

We employ probability distribution mathematics to predict how far a photon packet can propagate within the medium between interactions [8]. The probability density function of the pathlength ( $t$ ), also known as the step-size, between interactions or events is [9]

$$p(t) = \mu_t e^{-\mu_t t} \quad (1.5)$$

Solving for  $t$  in Eq. (1.5), we get

$$t = -\frac{\ln \xi}{\mu_t} \quad (1.6)$$

where  $\xi$  is random number between 0 and 1 sampled over a uniform distribution [9, 10]. Once the initial step size is calculated, we update the current position of the photon packet:

$$x' = r \cos(2\pi\beta) \quad (1.7)$$

$$y' = r \sin(2\pi\beta) \quad (1.8)$$

$$z' = t \quad (1.9)$$

A photon packet is launched a distance  $t$  into the medium where it has its first interaction. At this point, the model removes some of the weight from the photon packet due to absorption and scattering. The fraction of weight that is absorbed is

$$absorbed = \frac{\mu_a}{\mu_a + \mu_s} = \frac{\mu_a}{\mu_t} \quad (1.10)$$

which means that the new weight of the photon packet is reassigned a value of

$$w' = w - w \times absorbed = w(1 - absorbed) \quad (1.11)$$

where  $w$  is the previous photon packet weight, and  $w'$  is the new photon packet weight [10]. This reduced-weight photon packet is also scattered at the same point.

Next, we calculate a new step size just as we did in Eq. (1.6) except with a newly generated random number  $\xi$ . The new direction of propagation due to scattering from the event is defined by choosing a deviation from the previous direction of propagation. The azimuthal component  $\psi$  of this direction is distributed uniformly between 0 and  $2\pi$  because of the symmetry of the problem



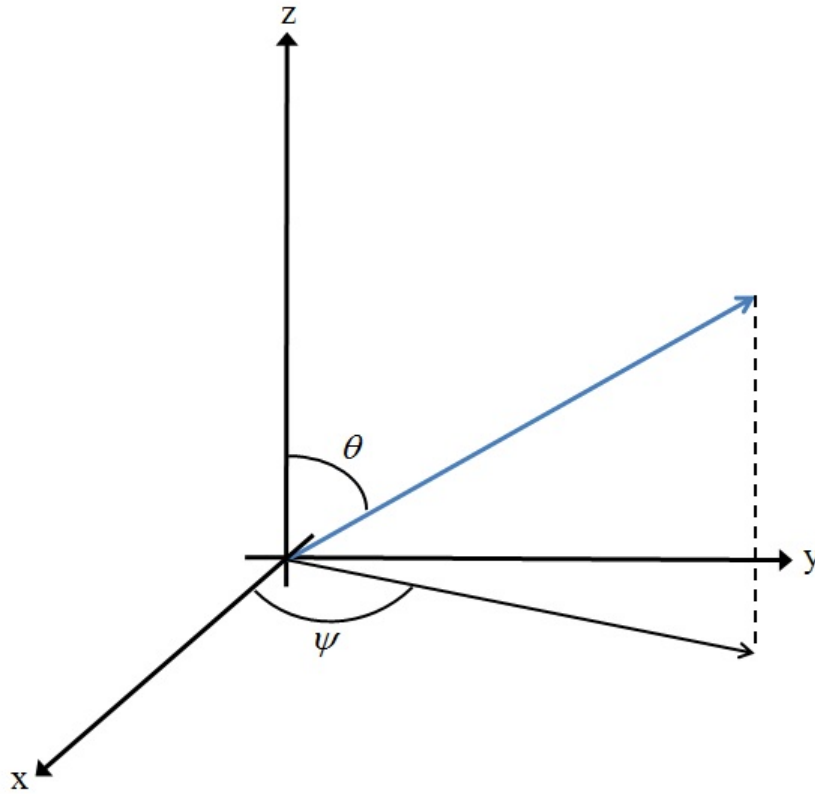


**Figure 1.1** Coordinate System for Scattering Angle

(infinite in  $x$  and  $y$ ). Therefore, we can generate this angle by multiplying  $2\pi$  by the uniformly distributed random number  $\xi$  used in calculating the step size [10]:

$$\psi = 2\pi\xi \quad (1.12)$$

The polar angle  $\theta$  is determined using the Henyey-Greenstein phase function, originally used for galactic scattering, which is given by

$$\cos \theta = \frac{1}{2g} \left( 1 + g^2 - \left( \frac{1 - g^2}{1 - g + 2g\xi} \right)^2 \right) \quad (1.13)$$

where  $g$  is the anisotropy factor [10]. The anisotropy factor  $g$  has a value between -1 and 1. A value near -1 represents backward-directed scattering (primarily reflective), 0 represents isotropic

scattering, and a value near 1 represents forward-directed scattering (primarily refractive) [8]. In the special case of  $g = 0$ , the polar angle  $\theta$  is instead determined by [10]

$$\cos \theta = 2\xi - 1 \quad (1.14)$$

Hence, for  $g = 0$ , reflective and refractive scattering are equally represented. We use the scattering angles  $\psi$  and  $\theta$  to find the directional cosines of the new direction:

$$\begin{aligned} \delta'_x &= \frac{\sin \theta}{\sqrt{1 - \delta_z^2}} (\delta_x \delta_z \cos \psi - \delta_y \sin \psi) + \delta_x \cos \theta \\ \delta'_y &= \frac{\sin \theta}{\sqrt{1 - \delta_z^2}} (\delta_y \delta_z \cos \psi + \delta_x \sin \psi) + \delta_y \cos \theta \\ \delta'_z &= -\sin \theta \cos \psi \sqrt{1 - \delta_z^2} + \delta_z \cos \theta \end{aligned} \quad (1.15)$$

where  $\delta_x$ ,  $\delta_y$ , and  $\delta_z$  are the previous directional cosines in the  $x$ ,  $y$ , and  $z$  directions, respectively [10]. If the polar angle is close to the normal, that is  $|\delta_z| > 0.99999$ , then the new directional cosines are determined by

$$\begin{aligned} \delta'_x &= \sin \theta \cos \psi \\ \delta'_y &= \sin \theta \sin \psi \\ \delta'_z &= \frac{\delta_z}{|\delta_z|} \cos \psi \end{aligned} \quad (1.16)$$

[10]. Directional cosines of photon packets start with

$$\begin{aligned} \delta_x &= 0 \\ \delta_y &= 0 \\ \delta_z &= -1 \end{aligned} \quad (1.17)$$

because the photon packet was initially launched normal to the interface. Once we have the directional cosines and the new step-size  $t$ , we move the photon packet to a new location  $(x', y', z')$ . This location is found from

$$\begin{aligned}x' &= x + \delta'_x t \\y' &= y + \delta'_y t \\z' &= z + \delta'_z t\end{aligned}\tag{1.18}$$

[10]. This procedure of moving the photon packet to the next scattering event, removing weight from the photon packet's current weight, determining a new step-size and scattering direction, and moving the photon packet again to the next event continues until the photon packet's weight becomes very small.

Eventually, the photon packet's weight may diminish to a point where it becomes very small before it leaves the tissue. Since only fractions of the photon packet's weight is taken off at each step, the weight will never reach zero but it will get very small. In order to be computationally efficient in the simulation, we eliminate packets with small weights using a Russian Roulette technique. Simply eliminating a packet completely because its weight falls below a threshold value,  $\zeta$ , would violate conservation of energy since this assumes that all of the energy was absorbed, which is not necessarily the case. To cleanly terminate photon packets, a Russian Roulette game is played with the photon packet: If the packet's weight falls below a certain value, then it has the chance of either surviving and propagating further to the next event or not surviving and becoming eliminated. The decision of whether or not a photon packet survives is statistically based [8]. We give the photon packet a probability  $1/N$  and choose  $N = 10$  that it will survive. A random number  $\varepsilon$  is chosen and compared to  $1/N$ . If  $\varepsilon > 1/N$ , then the photon packet dies, meaning it is reassigned a weight of  $w = 0$  and it stops propagating. If  $\varepsilon < 1/N$ , then the photon packet survives, meaning it is reassigned a new weight of  $w' = w \times N$  and it propagates to the next event. The

reassigning of weight to the surviving photon packet provides a statistical bias to the absorption of the sub-threshold photon packet's intensity. We can think of splitting the photon packet into  $N$  individual photon sub-packets, each of weight  $W/N$  [12]. Since we give the entire photon packet a probability of  $1/N$  of surviving, it's the same as saying 1 sub-packet out of  $N$  survives, and the other  $N - 1$  do not. Instead of throwing away all of the weight from the  $N - 1$  sub-packets into absorption, we give the 1 surviving sub-packet the weight from these  $N - 1$  dying sub-packets. If we average this reassigning weight over all photon packets that propagate through the medium, statistically, we could reassign the weight of a surviving photon packet the weight of the other photon packets that died or will die, thus assigning it a weight of  $w' = w \times N$ . This process satisfies conservation of energy since absorption events always extract a portion of the energy but never all.

Finally, the observable quantities of reflectance, transmittance, absorption, and energy are calculated and determined [8]. In our simulations, we focus on the amount of intensity from the photon packets that hits the detector region.

### 1.3 Modified Beer's Law

Beer's law, also known as the Beer-Lambert law, is used to describe the absorption of light in non-scattering media. It is given as

$$I(d) = I_0 e^{-\epsilon cd}, \quad (1.19)$$

where  $I_0$  is the intensity of light emitted from the source,  $\epsilon$  is molar absorptivity,  $c$  is molar concentration, and  $d$  is the physical separation of the light source and detector [11].

When the material of interest is a heavy scatterer, such as tissue, Beer's law must be adjusted for the scattering paths that the light takes. A modified form of Beer's law is

$$I(d) = I_0 e^{-\alpha d}, \quad (1.20)$$

where  $I_0$  and  $d$  have the same definitions above, and

$$\alpha = \sqrt{3\mu_a(\mu_a + \mu'_s)} \quad (1.21)$$

is the bulk attenuation coefficient of the tissue sample [11]. Coefficients  $\mu_a$  and  $\mu'_s$  are the absorptive and reduced scattering coefficients, respectively [11]. The reduced scattering coefficient  $\mu'_s$  can be written in terms of the scattering coefficient  $\mu_s$  and anisotropy factor  $g$  [11]

$$\mu'_s = (1 - g)\mu_s \quad (1.22)$$

One can see that in the limit of  $\mu'_s \ll \mu_a$ , the modified form of Beer's law approaches the original Beer's Law in that it is no longer dependent on scattering but instead solely on absorption:

$$\lim_{\mu'_s \rightarrow 0} I(d) = \lim_{\mu'_s \rightarrow 0} I_0 e^{-\alpha d} \quad (1.23)$$

$$= \lim_{\mu'_s \rightarrow 0} I_0 e^{-\sqrt{3\mu_a(\mu_a + \mu'_s)}d} \quad (1.24)$$

$$= I_0 e^{-\sqrt{3}\mu_a d} \quad (1.25)$$

# Chapter 2

## Methods and Procedures

We ran semi-infinite models (finite in  $z$ , infinite in  $x$  and  $y$ ) of pure material, layered material, and homogeneous mixed material using Mathematica. The materials modeled were a few basic constituents of the human finger: epidermis, water, and whole blood, each illuminated by a collimated beam of monochromatic light at  $\lambda = 810$  nm and simulated with 500 photon packets. We ran each simulation starting at a thickness  $d$  of 0.010 mm increasing in increments of 0.100 mm up to a maximum thickness of 5.01 mm. We then plotted the transmitted intensity collected in the detector region versus thickness,  $d$ , and fit it with an exponential decay curve to derive a decay constant,  $\alpha$ . The decay constant in the exponential was then compared to the  $\alpha$  given in Eq. (1.20) for the respective tissues. It was important to run each simulation set up to a thickness  $\geq 2 - 3$  mm to yield a proper exponential decay relation that can be fit to the data.

## 2.1 Development of Monte Carlo Simulation for Semi-Infinite Pure Tissue Model and Comparison to Previously Published Results

We first modeled semi-infinite pure tissue structures of epidermis, water, and whole blood, separately. These simulations successfully modeled the change in detected intensity versus the thickness of the sample for a modified form of Beer's Law in materials that exhibit high scattering properties (see Eq. (1.20) and Figs. 2.3-2.5):

The derived  $\alpha$  values agree with published values from diffusion models after they are normalized to our approach by dividing out the  $\sqrt{3}$  factor in Eq. (1.21) (see Table 2.1).

Material	$\mu_a$ ( $\text{mm}^{-1}$ )	$\mu_s$ ( $\text{mm}^{-1}$ )	$\mu_t$ ( $\text{mm}^{-1}$ )	$g$	$\alpha_{normalized}$ ( $\text{mm}^{-1}$ )	$\alpha_{derived}$ ( $\text{mm}^{-1}$ )
epidermis	4.0	42.0	46.0	0.85	6.419	7.815
water	$2.0 \times 10^{-3}$	$3.0 \times 10^{-7}$	$2.0003 \times 10^{-3}$	0.9	$2.0 \times 10^{-3}$	$1.14 \times 10^{-3}$
whole blood	0.65	69.0	69.65	0.989	0.957	0.931

**Table 2.1** Absorption ( $\mu_a$ ), scattering ( $\mu_s$ ), transmission ( $\mu_t$ ), and bulk attenuation ( $\alpha$ ) coefficients and anisotropy factor ( $g$ ) of epidermis [11], water [13], and whole blood (Hct=0.45-0.46, oxygenation>98%) [11] at a wavelength of 810 nm. The values for  $\alpha_{normalized}$  are the values calculated using Eq. (1.21), normalized by dividing out the  $\sqrt{3}$ . The values for  $\alpha_{derived}$  are the attenuation coefficients we obtained from fitting an exponential decay to the results from the simulations (see Fig. 2.3). Comparing  $\alpha_{normalized}$  to  $\alpha_{derived}$ , we see that the two values agree quite well.

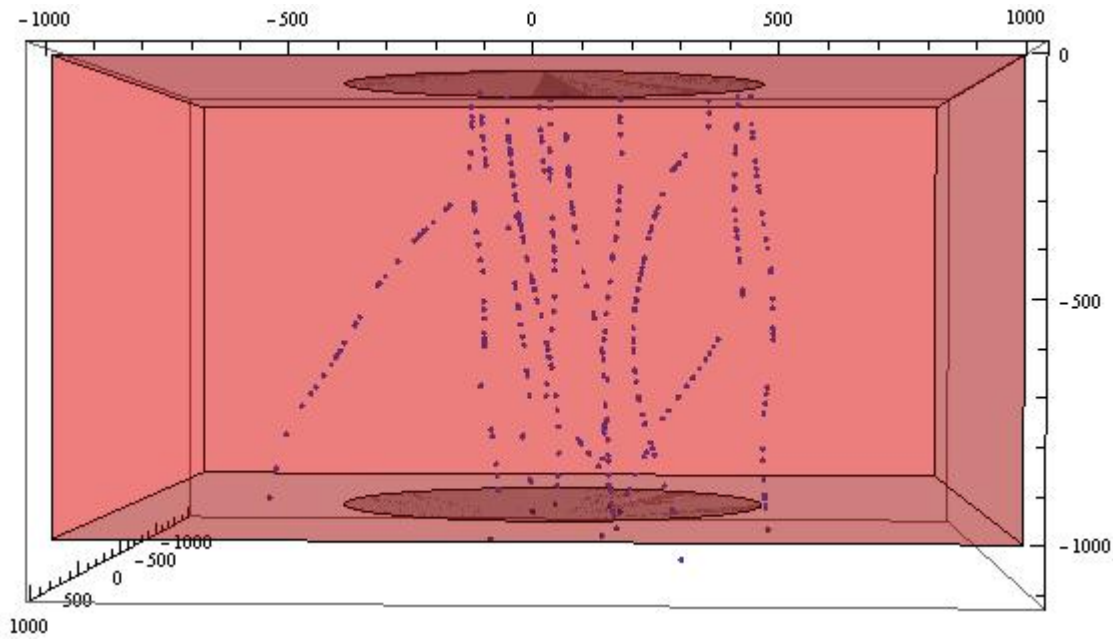


**Figure 2.1** Paths are traced of 10 photon packets in Monte Carlo simulation for a semi-infinite slab of blood. The source is at the top, centered at the origin, while the detector is at the bottom, centered at  $(0,0,1 \text{ mm})$ .



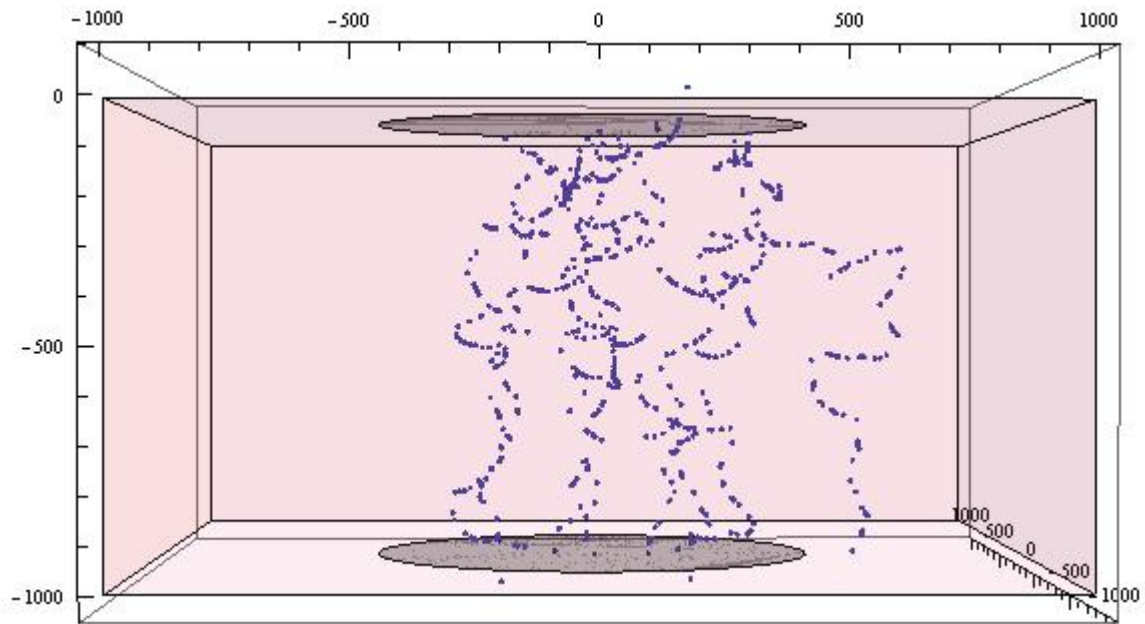


**Figure 2.2** Paths are traced of 10 photon packets in Monte Carlo simulation for a semi-infinite slab of epidermis. The source is at the top, centered at the origin, while the detector is at the bottom, centered at  $(0, 0, 1 \text{ mm})$ .

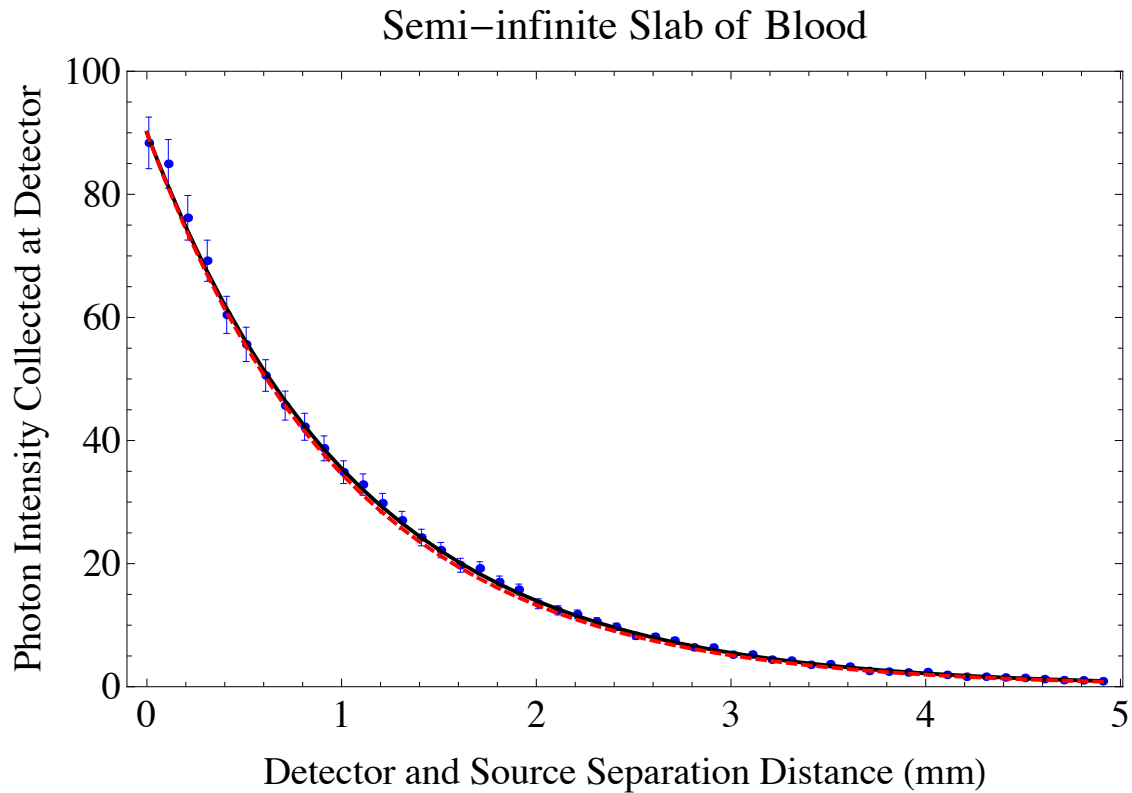


**Figure 2.3** Results of the Monte Carlo simulation for a semi-infinite slab of whole blood, represented by solid blue points. Error bars from Poisson statistics are smaller than most data symbols. The modeled attenuation coefficient  $\alpha_{derived}$  is derived from the solid black curve, and substituting the theoretical normalized value,  $\alpha_{normalized}$ , into modified Beer's law, Eq. (1.20) gives the dashed red line. One can see that the derived exponential decay curve of the data (solid black) is in good agreement with the modified form of Beer's Law and Eq.(1.21) (dashed red).

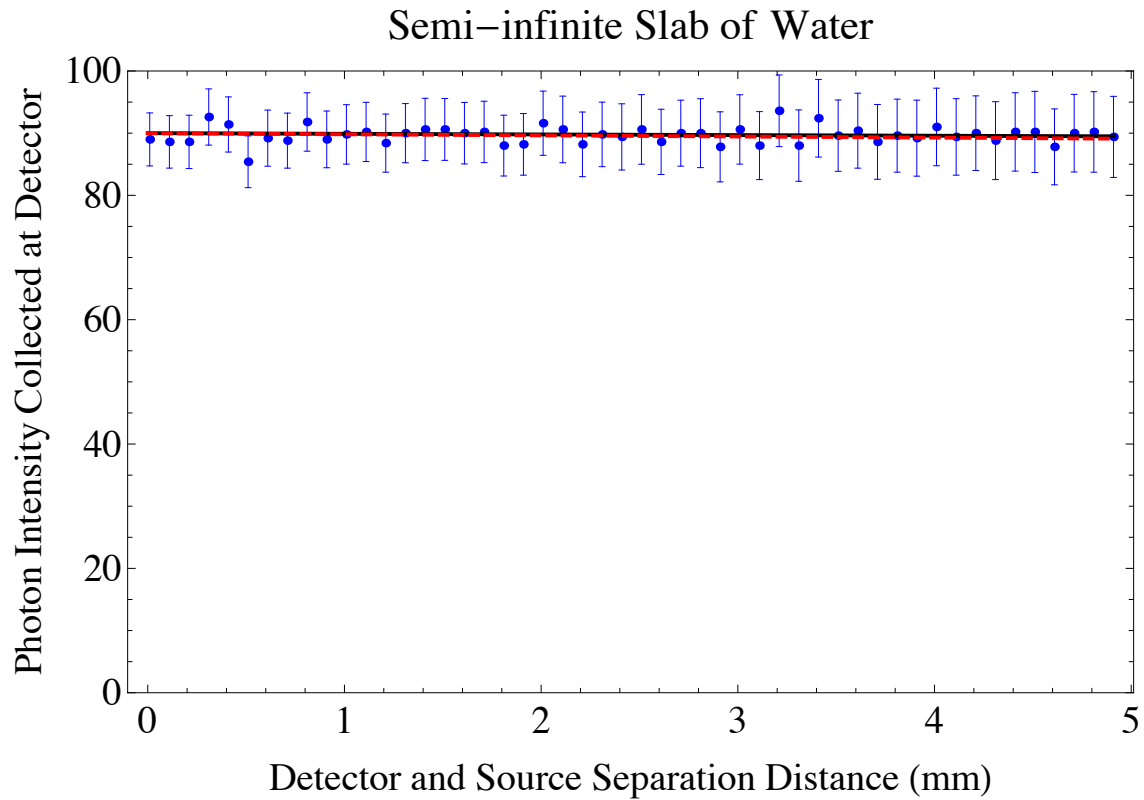


**Figure 2.4** Results of the Monte Carlo simulation for a semi-infinite slab of water, represented by solid blue points. Error bars from Poisson statistics are shown. The modeled attenuation coefficient  $\alpha_{derived}$  is derived from the solid black curve, and substituting the theoretical normalized value,  $\alpha_{normalized}$ , into modified Beer's law, Eq. (1.20) gives the dashed red line. One can see that the derived exponential decay curve of the data (solid black) is in good agreement with the modified form of Beer's Law and Eq.(1.21) (dashed red).

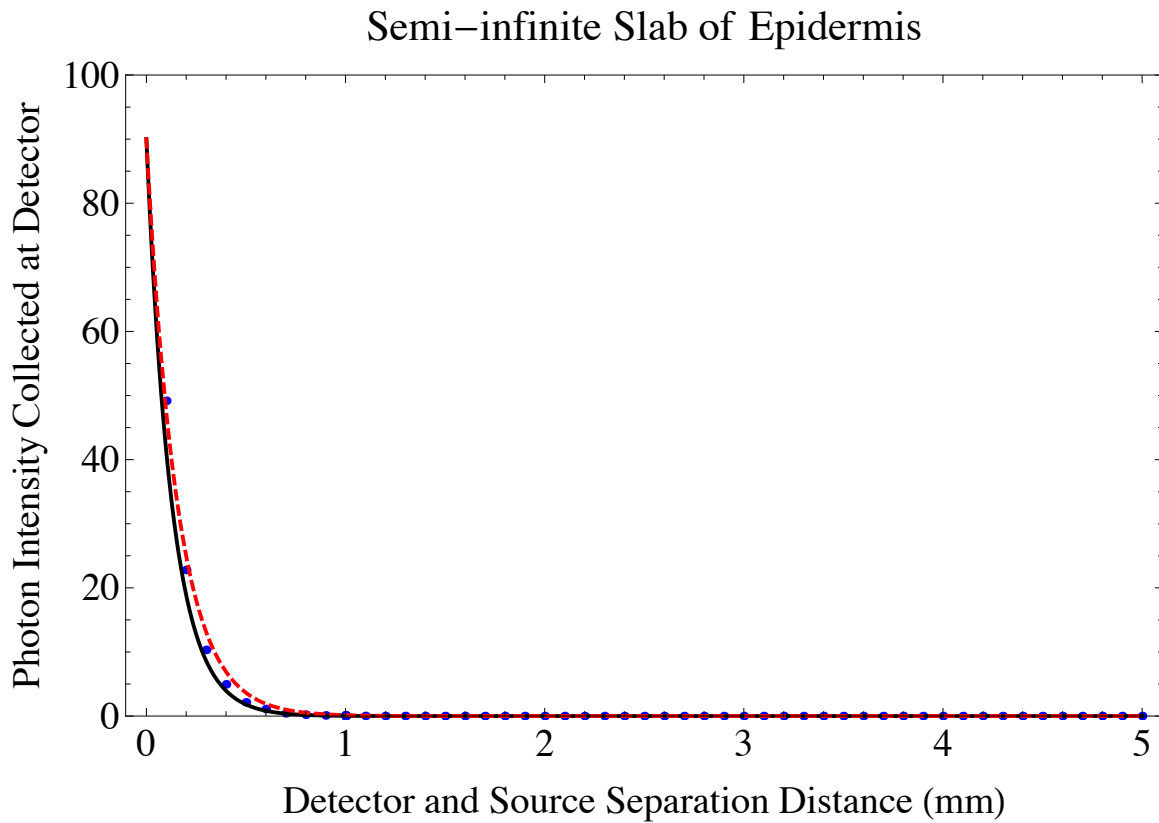


**Figure 2.5** Results of the Monte Carlo simulation for a semi-infinite slab of epidermis, represented by solid blue points. Error bars from Poisson statistics are smaller than most data symbols. The modeled attenuation coefficient  $\alpha_{derived}$  is derived from the solid black curve, and substituting the theoretical normalized value,  $\alpha_{normalized}$ , into modified Beer's law, Eq. (1.20) gives the dashed red line. One can see that the derived exponential decay curve of the data (solid black) is in good agreement with the modified form of Beer's Law and Eq.(1.21) (dashed red).

## 2.2 Development of Monte Carlo Simulation for Semi-Infinite Layered Tissue Model and Comparison to Previously Published Results

We next modeled layers of two different types of materials. This was accomplished by dividing up a semi-infinite volume (finite in  $z$ , infinite in  $x$  and  $y$ ) into two separate layers, each composed of a different material. The interface between the two layers was given a specific coordinate, say  $z_1$ . The model took careful consideration of how a photon packet interacted at this interface. Since we placed the source and detector within the semi-infinite material of interest, directly at the top and bottom, we neglected the interface between the two layers for when there was 0% of the top layer or 0% of the bottom layer, meaning there was just one layer. Thus, we did not have to handle the possibility of reflection at the interface for those two cases. Furthermore, when the next step-size took the photon packet across the interface, we utilized Snell's law to change the direction of propagation and also readjusted the length of the remaining step size to accommodate the differing scattering and absorptive properties of the material the photon has entered.

Snell's law is given by

$$\begin{aligned} n_1 \sin \theta_1 &= n_2 \sin \theta_2 \\ \sin \theta_2 &= \frac{n_1}{n_2} \sin \theta_1 \end{aligned} \tag{2.1}$$

where  $n_1$  is the index of refraction of the material the photon packet was first in,  $\theta_1$  is the angle of incidence to the boundary between the two materials (measured from the normal),  $n_2$  is the index of refraction of the material that the photon packet is traveling to, and  $\theta_2$  is the angle of transmittance through the boundary between the two materials (measured from the normal). As applied to absorbing materials, Snell's law usually requires a complex index of refraction. However, in the

Material	n
epidermis	1.42
water	1.33
whole blood	1.37

**Table 2.2** Indices of refraction of epidermis [14], water [15], and whole blood [16].

case of the materials we are working with, the imaginary part of the index of refraction for each material is small enough that we can neglect it. Thus, using simple Snell’s law is sufficient at the boundary between layers.

If the condition for the critical angle is exceeded, that is

$$\frac{n_1}{n_2} \sin \theta_1 \geq 1 \tag{2.2}$$

then the photon packet reflects back into the material that it was originally in at an angle  $\theta_{new} = -\theta_1$ .

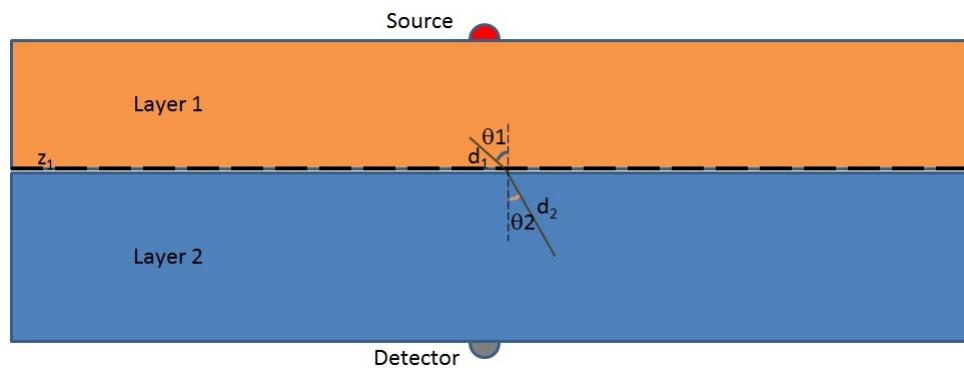


**Figure 2.6** Semi-infinite layered model for two tissue layers

Rescaling the remaining step-size of the photon packet past the boundary was accomplished simply by returning to the equation for step size (1.6). First, we found how much of the step-size

in the  $z$ -direction the photon packet travels in the first medium and use it to find a scaling factor for the distances it travels in the  $x$ -,  $y$ - and  $z$ -directions:

$$scale = \frac{z_1 - z}{t \times \delta_z} \quad (2.3)$$

$$t_1 = t \times scale \quad (2.4)$$

$$x_1 = x + \delta_x t_1 \quad (2.5)$$

$$y_1 = y + \delta_y t_1 \quad (2.6)$$

$$z_1 = z + \delta_z t_1 \quad (2.7)$$

$$(2.8)$$

In the above equations,  $z_1$  is the location in the  $z$ -direction of the boundary between the two materials;  $(x, y, z)$  is the current location of the photon packet before it takes its step;  $\delta_x$ ,  $\delta_y$ ,  $\delta_z$  are directional cosines (see Section 1.2);  $t$  is the original step-size; and  $t_1$  is the step-size the photon packet takes in the first medium. By performing these calculations, the photon packet will be placed at the boundary.

If the photon packet is scattered into the next medium, then the new scattering angle is determined by Snell's law. Next we determine if the photon packet is reflected at the boundary or transmitted into the next medium. We accomplish this using Fresnel's formula for the probability of reflection [8]. The Fresnel coefficients for  $s$ -polarized light and  $p$ -polarized light, respectively, are [17]

$$r_s = -\frac{\sin(\theta_i - \theta_t)}{\sin(\theta_i + \theta_t)} \quad (2.9)$$

$$r_p = -\frac{\tan(\theta_i - \theta_t)}{\tan(\theta_i + \theta_t)} \quad (2.10)$$

The fraction of light reflected from the boundary is given by

$$R_s = |r_s|^2 \quad (2.11)$$

$$= \frac{\sin^2(\theta_i - \theta_t)}{\sin^2(\theta_i + \theta_t)} \quad (2.12)$$

$$R_p = |r_p|^2 \quad (2.13)$$

$$= \frac{\tan^2(\theta_i - \theta_t)}{\tan^2(\theta_i + \theta_t)} \quad (2.14)$$

for  $s$ -polarized and  $p$ -polarized light, respectively [17]. Since we assume that the light has no particular polarization, we average the two equations above for the two orthogonal polarization directions [8]:

$$R(\theta_i) = \frac{1}{2} \left[ \frac{\sin^2(\theta_i - \theta_t)}{\sin^2(\theta_i + \theta_t)} + \frac{\tan^2(\theta_i - \theta_t)}{\tan^2(\theta_i + \theta_t)} \right] \quad (2.15)$$

We generate a random number  $\rho$  and compare it to the Fresnel formula above with the respective  $\theta_i$  and  $\theta_t$  substituted in. If  $\rho \leq R(\theta_i)$  then the photon packet is reflected and remains at the boundary with the directional cosines updated to  $(\delta'_x, \delta'_y, \delta'_z) = (\delta_x, \delta_y, -\delta_z)$ . If  $\rho > R(\theta_i)$ , then the photon packet is transmitted into the next medium. The remaining step size is found by subtracting the first step to the boundary from the total step size, and then rescaling due to a difference in transmission coefficients:



$$t_2 = (t - t_1) \times \frac{\mu_{t,1}}{\mu_{t,2}} \quad (2.16)$$

$$\sin \theta' = \frac{n_1}{n_2} \sin \theta \quad (2.17)$$

$$x = x_1 + \sin \theta' \cos \psi t_2 \quad (2.18)$$

$$y = y_1 + \sin \theta' \sin \psi t_2 \quad (2.19)$$

$$z = z_1 + \cos \theta' \text{Sign}(\delta_z) t_2 \quad (2.20)$$

$$(2.21)$$

where  $\mu_{t,1}$  is the transmission coefficient for the first medium,  $\mu_{t,2}$  is the transmission coefficient for the new medium,  $n_1$  is the refractive index for the first medium,  $n_2$  is the refractive index for the new medium, and  $(x, y, z)$  is the final location of the photon packet for this particular event.

We first simulated a layered model of water and whole blood with water being the top layer and blood being the lower layer. The simulation proved accurate with models consisting of 100% water (see Fig. 2.4 and Table 2.1) or 100% blood (see Fig. 2.3 and Table 2.1). The curve for intensity vs. thickness of material followed the same modified Beer's Law form that we saw previously in a homogeneous model, as expected.

We next changed the composition of the semi-infinite slab to consist of various volume fractions of water and blood (e.g. 10% of the volume being water with the other 90% being blood) and generated the same intensity vs. thickness curves as before. Once again, there was an exponential decay form of the function that followed the modified form of Beer's Law. We fit a decay constant  $\alpha$  to each of these curves. Then, we compared them on a graph that represents the total  $\alpha$  vs. the volume fraction of water (see Fig. 2.9 and 2.8). One would expect there to be a linear relationship between  $\alpha$  and the volume fraction of water based on simple multiplication of exponential decay curves. That is, let  $d_1$  be the thickness of the layer of water,  $d_2$  be the thickness of the layer of blood,  $\alpha_{water}$  be the attenuation coefficient of water,  $\alpha_{blood}$  be the attenuation coefficient of blood,

$x$  be the fraction of the total volume that is water, and  $y$  be the fraction of the total volume that is blood. Thus, we see that

$$\begin{aligned}
 I(d_1, d_2) &= I_0 e^{-\alpha_{\text{water}} d_1} e^{-\alpha_{\text{blood}} d_2} \\
 I(d) &= I_0 e^{-(\alpha_{\text{water}} x d + \alpha_{\text{blood}} y d)} \\
 I(d) &= I_0 e^{-(\alpha_{\text{water}} x + \alpha_{\text{blood}} y) d} \\
 I(d) &= I_0 e^{-(\alpha_{\text{water}} x + \alpha_{\text{blood}} (1-x)) d} \\
 I(d) &= I_0 e^{-\alpha_{\text{total}} d}
 \end{aligned} \tag{2.22}$$

where  $\alpha_{\text{total}} = \alpha_{\text{water}} x + \alpha_{\text{blood}} y = \alpha_{\text{water}} x + \alpha_{\text{blood}} (1-x)$  and  $x + y = 1$ . From our simulations, we were able to produce the linear relationship between  $\alpha_{\text{total}}$  and the volume fraction of water.

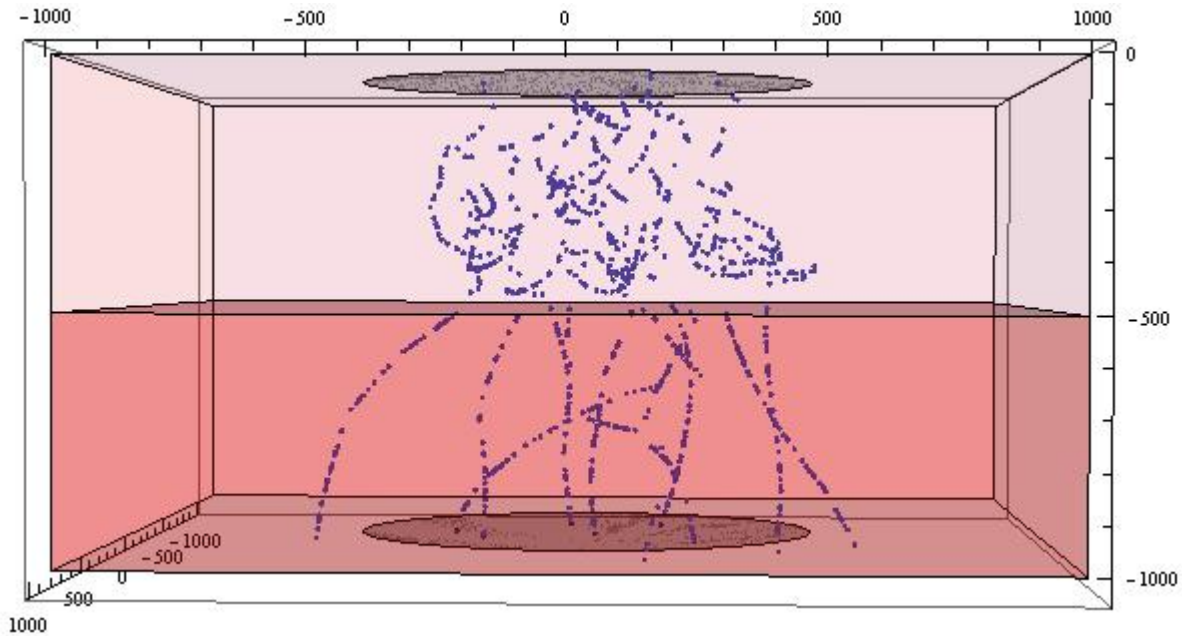


**Figure 2.7** Paths are traced of 10 photon packets in Monte Carlo simulation for a semi-infinite layered slab of 1/2 epidermis (top layer) and 1/2 blood (bottom layer). The source is at the top, centered at the origin, while the detector is at the bottom, centered at (0, 0, 1 mm).

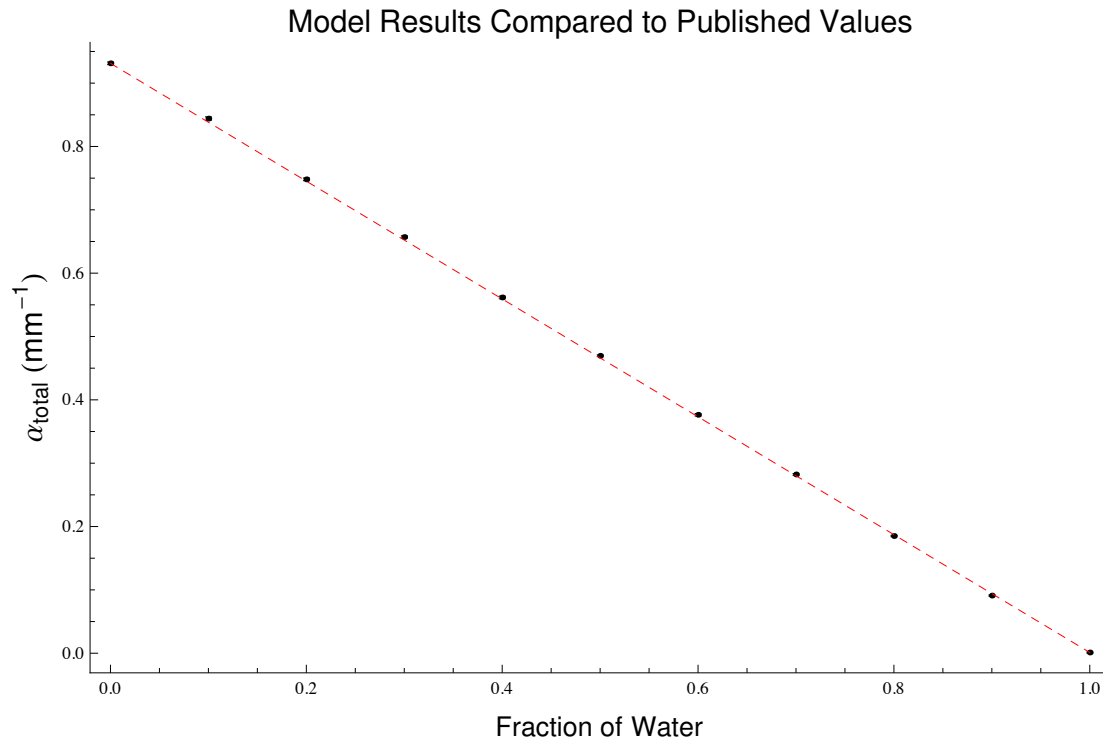


**Figure 2.8** Bulk attenuation coefficient  $\alpha$  as a function of volume fraction of water in a layered model of water as the layer near the source and blood as the layer near the detector. Statistical error bars are shown for each point, but are too small to see for most points. The coefficient of determination,  $R^2$ , is the statistical value that represents how close the data points follow the linear relationship between  $\alpha$  and the volume fraction of water (dashed line). The results for this model yield  $R^2 = 1.0 \pm 10^{-4}$ . A value of  $R^2 = 1$  represents a perfect correlation.

When we flipped the order of the layers such that blood was the upper layer and water was the lower layer, we found that there was a large amount of noise in the results for the detected intensity as a function of thickness of material (see Fig. 2.9). Thus, we were unable to produce as clean a linear relationship for  $\alpha$  as a function of volume fraction of blood as we saw above (see Fig. 2.8). The main reason for this increase in noise is that very little intensity from the photon packets is reaching the detector. Since the index of refraction of blood is higher than that of water (see Table 2.2), and the upper layer is composed of blood, most photon packets that hit the blood-water interface in the simulation are reflected back into the blood layer because of the condition Eq.

(2.2).

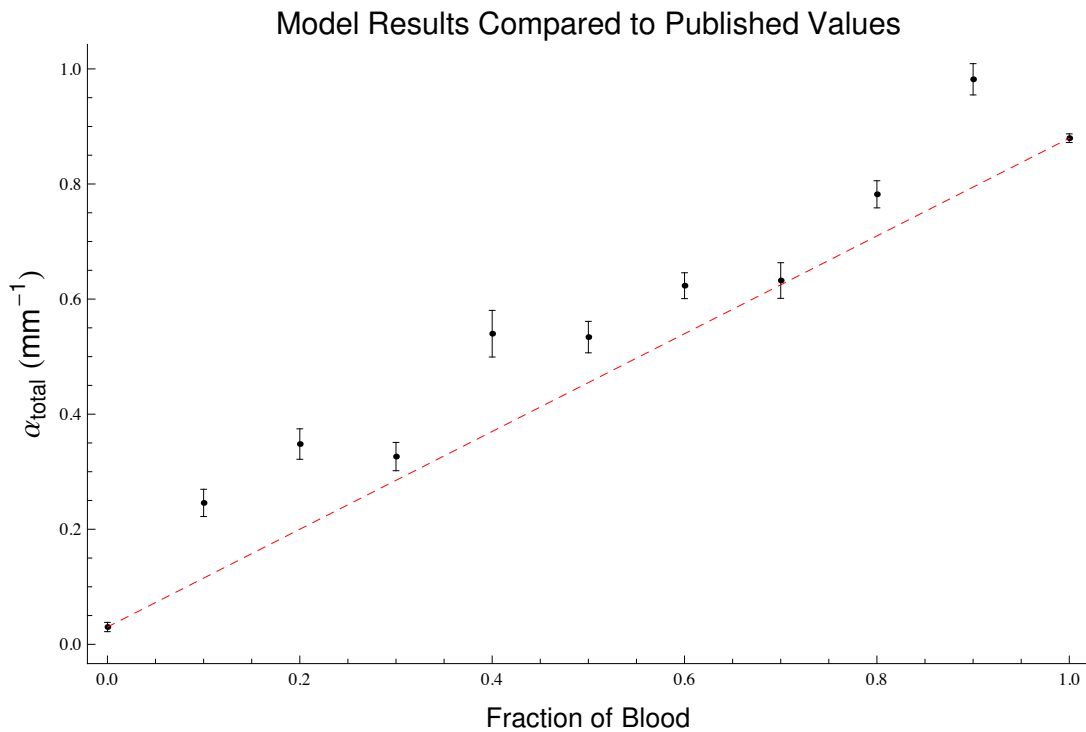


**Figure 2.9** Bulk attenuation coefficient  $\alpha$  as a function of volume fraction of blood in a layered model of blood then water. Statistical error bars are shown for each point and are large for this model due to noise from reflection at the blood-water interface. The coefficient of determination,  $R^2$ , is the statistical value that represents how close the data points follow the linear relationship between  $\alpha$  and the volume fraction of blood (dashed line). The results for this model yield  $R^2 = 0.849$ . A value of  $R^2 = 1$  represents a perfect correlation.

Replacing water with epidermis and running the simulations with epidermis as the top layer and blood as the lower layer and vice-a-versa, there was a linear relationship between the volume fraction of either substance and the total attenuation coefficient. Just as happened in the previous case with a layered model of blood and water, the configuration in which blood was the top layer (see Fig. 2.11) yielded noisy results.

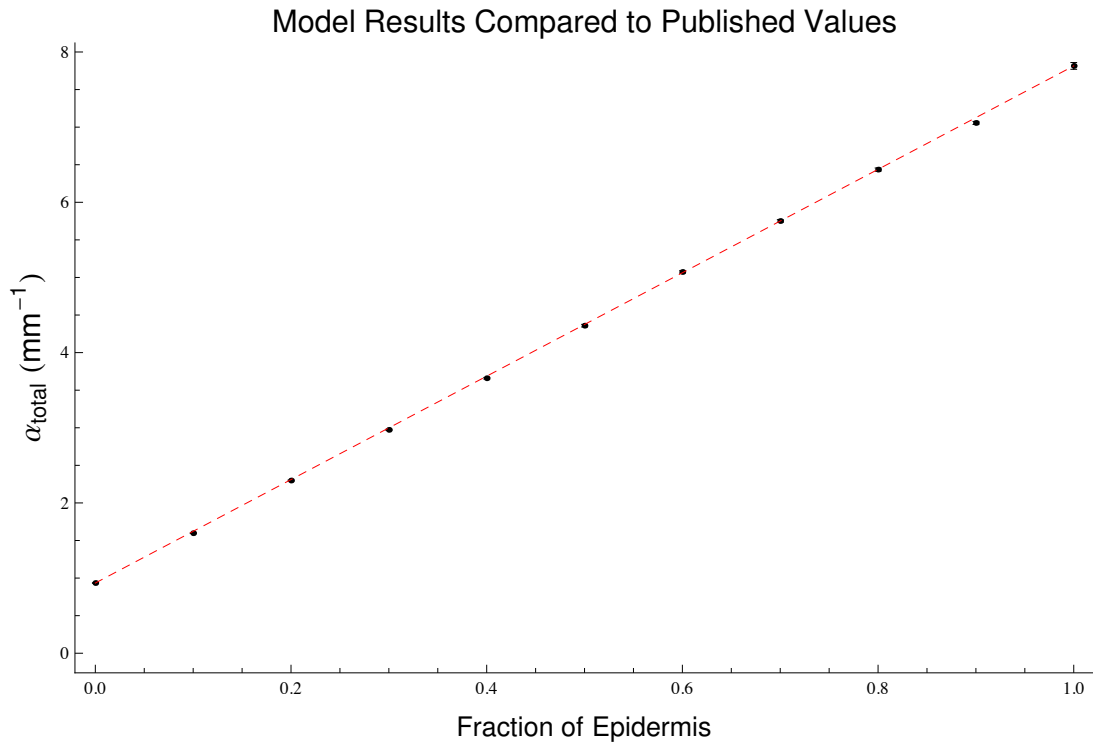


**Figure 2.10** Bulk attenuation coefficient  $\alpha$  as a function of volume fraction of epidermis in a layered model of epidermis, then blood. Statistical error bars are shown for each point, but are too small to see for many points. The coefficient of determination,  $R^2$ , is the statistical value that represents how close the data points follow the linear relationship between  $\alpha$  and the volume fraction of epidermis (dashed line). The results for this model yield  $R^2 = 1.0 \pm 10^{-4}$ . A value of  $R^2 = 1$  represents a perfect correlation.

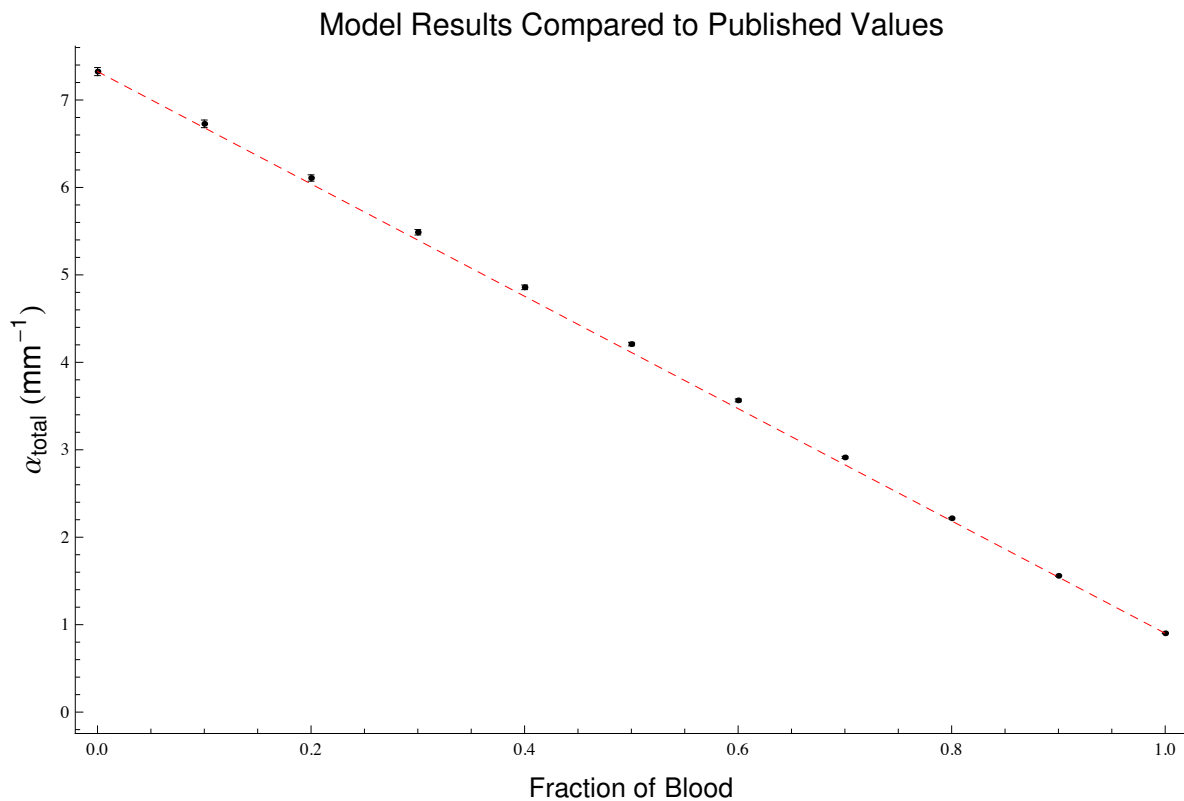


**Figure 2.11** Bulk attenuation coefficient  $\alpha$  as a function of volume fraction of blood in a layered model of blood then epidermis. Statistical error bars are shown for each point. The coefficient of determination,  $R^2$ , is the statistical value that represents how close the data points follow the linear relationship between  $\alpha$  and the volume fraction of water (dashed line). The results for this model yield  $R^2 = 0.999$ . A value of  $R^2 = 1$  represents a perfect correlation.

## 2.3 Development of Monte Carlo Simulation for Semi-Infinite Homogeneous Mixed Tissue Model

We took the models a step further and simulated the light propagation through a homogeneous mix (not layers) of two materials. The idea was to use a random number  $\eta$  between 0 and 1 to select which material the photon packets interacted with at each specific event. If the random number fell within a certain range, then, at that event, the photon packet interacts with one given material,

meaning the transmission, absorption, and scattering coefficients and the anisotropy factor for that given material are used in calculating the new weight of the photon packet, the next step size, and the new scattering angle. If the random number fell within another range, then the photon packet interacts with the other material, so the coefficients and anisotropy factor for that material were used. When the photon packet reached its next event, a new random number was generated, and the process was repeated.

In deciding which material was likely to interact with the photon packet, we had to use the "interaction volume" fraction rather than a simple volume fraction. At first, we tried basing the threshold range for selecting an interaction material on the volume fraction alone. For example, to model a photon interaction in a material where 10% of the particles was water and the other 90% was blood, the selection range for water would be 0 – 0.10 and the selection range for blood would be 0.10 – 1.00. If the random number  $\eta$  mentioned above fell within the water selection range, then we say that the photon packet interacted with water at that event; otherwise, it would interact with blood. However, this method in selecting which material the photon packet interacts with at each event did not produce accurate results because the interaction cross-sections of each material, which is related to  $\mu_t$ , differed from one another. The coefficient  $\mu_t$  relates to the interaction cross-section,  $\sigma$ , of a material as

$$\frac{\mu_t}{\rho} = \frac{N_A}{M} \sigma \quad (2.23)$$

$$\frac{\mu_t}{\rho} = \frac{\eta_t}{\rho} \sigma \quad (2.24)$$

where  $\rho$  is the mass density of the material,  $N_A$  is Avagadro's number,  $M$  is the molar mass of the material, and  $\eta_t$  is the number of target entities per unit volume ( $\text{m}^{-3}$ ) [18]. Since the interaction cross-section,  $\sigma$ , is directly related to  $\mu_t$ , and it must be rescaled in a material that is mixed together, we must also rescale  $\mu_t$ .

Previously, in the layered model, we related the total attenuation coefficient  $\alpha_{total}$  to the volume fraction composition of water and blood. No special considerations were required in this model as we divided the whole volume up into layers of the different materials. However, when we mixed different materials together, we needed to consider how the differing scattering and absorption properties are related to the interaction volumes of the different materials. To illustrate why, compare the Monte Carlo photons to a bouncy ball moving around in a volume of bowling balls and ping-pong balls with just enough space between the balls for the bouncy ball to move around the room.<sup>1</sup> The bowling balls represent particles of the material with higher scattering and absorption properties. The ping-pong balls represent particles of the material with lower scattering and absorption properties. Intuitively, it makes sense that as the bouncy ball moves around the volume, not only are the bowling balls going to absorb more energy than the ping-pong balls, but it is also more probable that the bouncy ball will hit a bowling ball rather than a ping-pong ball due to the difference in sizes, or interaction volumes, of the two balls.

Relating the simulation to the bowling-ball-ping-pong-ball analogy, if Material 2 has higher scattering and absorption properties (e.g. the bowling balls) than Material 1, then the photon packet is more likely to interact with Material 2 than Material 1. Thus, we re-scaled the selection windows of each material to represent the fraction that each material takes of the whole “interaction” volume.

The rescaling goes as follows: Let  $x$ ,  $y$ ,  $\mu_{t,1}$ , and  $\mu_{t,2}$  have the same definitions as mentioned above. To rescale the volume fraction to the interaction volume of each material in the mixed model, the “cut-off” for the window in selecting between the two materials is

---

<sup>1</sup>In this analogy, we relate a larger mass directly to attenuating the moving ball’s motion more. In reality, this is not the case, but we keep the analogy as an illustrative learning tool.



$$\text{cut-off} = \frac{x\mu_{t,1}}{x\mu_{t,1} + y\mu_{t,2}} \quad (2.25)$$

$$= \frac{x\mu_{t,1}}{x\mu_{t,1} + (1-x)\mu_{t,2}} \quad (2.26)$$

If the random number is between 0 and cut-off, then the photon packet interacts with Material 1, otherwise it interacts with Material 2.

Again, the propagation distance between interactions,  $t$ , given by Eq. (1.6) is also affected by the difference in interaction coefficients. The interaction coefficient,  $\mu_t$ , corresponds to the interaction cross-section of a material. A larger  $\mu_t$  corresponds to a larger interaction cross-section, and, in turn, a larger interaction volume. In our mixed tissue models,  $\mu_t$  was rescaled as a linear proration of the two materials. Thus, the new  $\mu_t$ ,  $\mu_{t,total}$ , has the form

$$\mu_{t,total} = x\mu_{t,1} + y\mu_{t,2}$$

$$\mu_{t,total} = x\mu_{t,1} + (1-x)\mu_{t,2}, \quad (2.27)$$

## Chapter 3

### Results and Conclusions

After making the adjustments above, we ran the simulation for a mixture of water and blood (see Fig. 3.3) and blood and epidermis (see Fig. 3.4). The results are plotted as  $\alpha_{total}$  vs. volume fraction. We found nonlinearities present in the homogeneous mixed model that were not seen in the layered model.

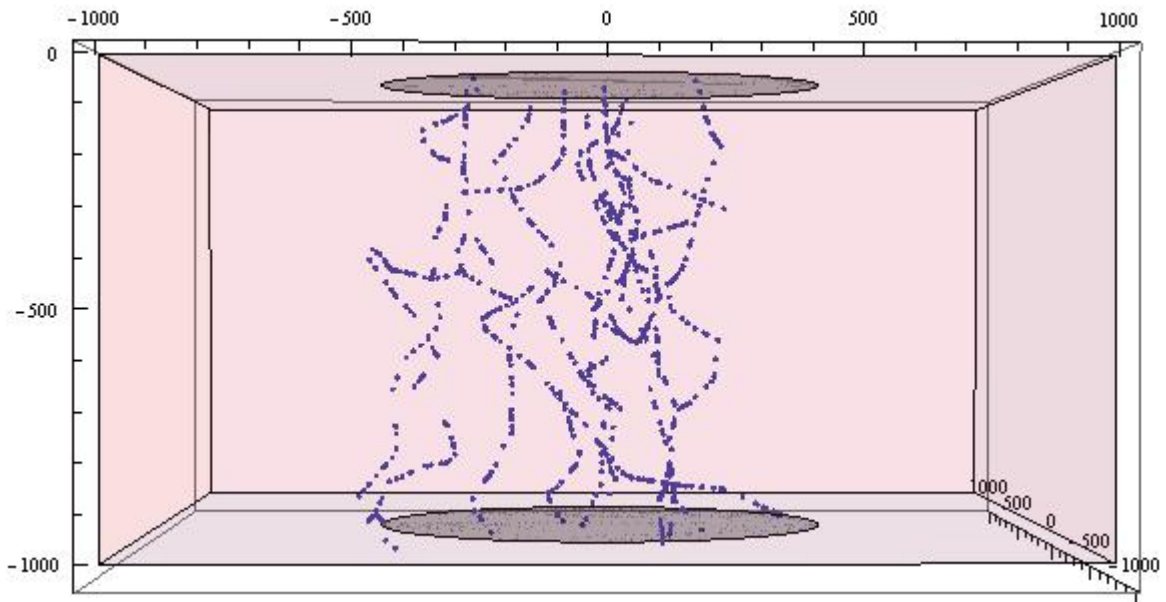


**Figure 3.1** Paths are traced of 10 photon packets in Monte Carlo simulation for a semi-infinite slab of a homogeneous mix of 50% epidermis and 50% blood. The source is at the top, centered at the origin, while the detector is at the bottom, centered at  $(0, 0, 1 \text{ mm})$ .

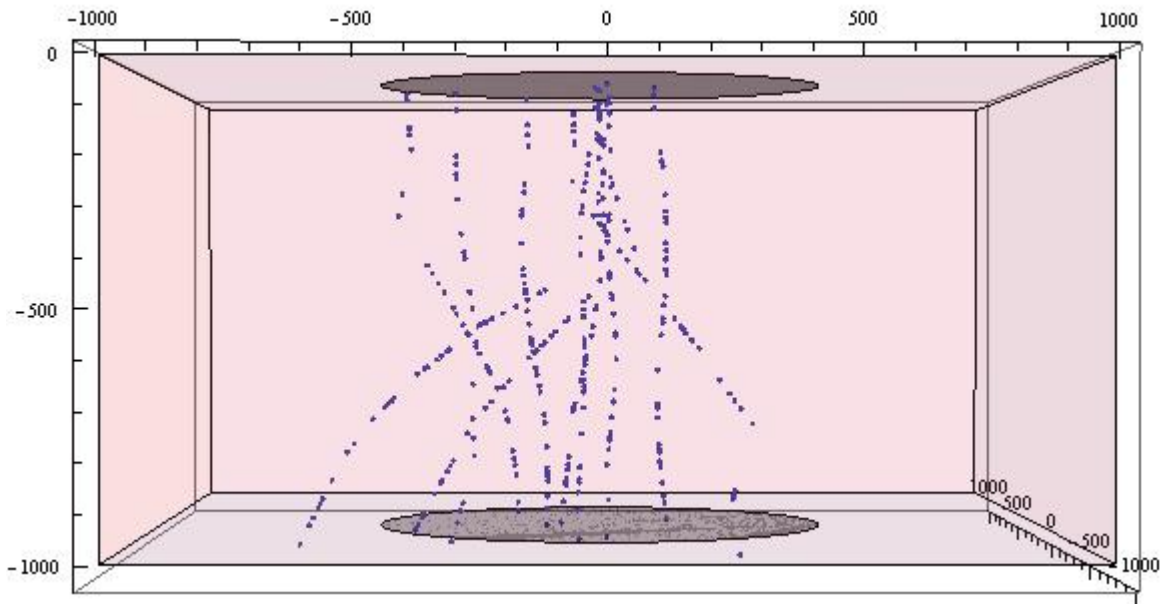


**Figure 3.2** Paths are traced of 10 photon packets in Monte Carlo simulation for a semi-infinite slab of a homogeneous mix of 50% water and 50% blood. The source is at the top, centered at the origin, while the detector is at the bottom, centered at  $(0, 0, 1 \text{ mm})$ .

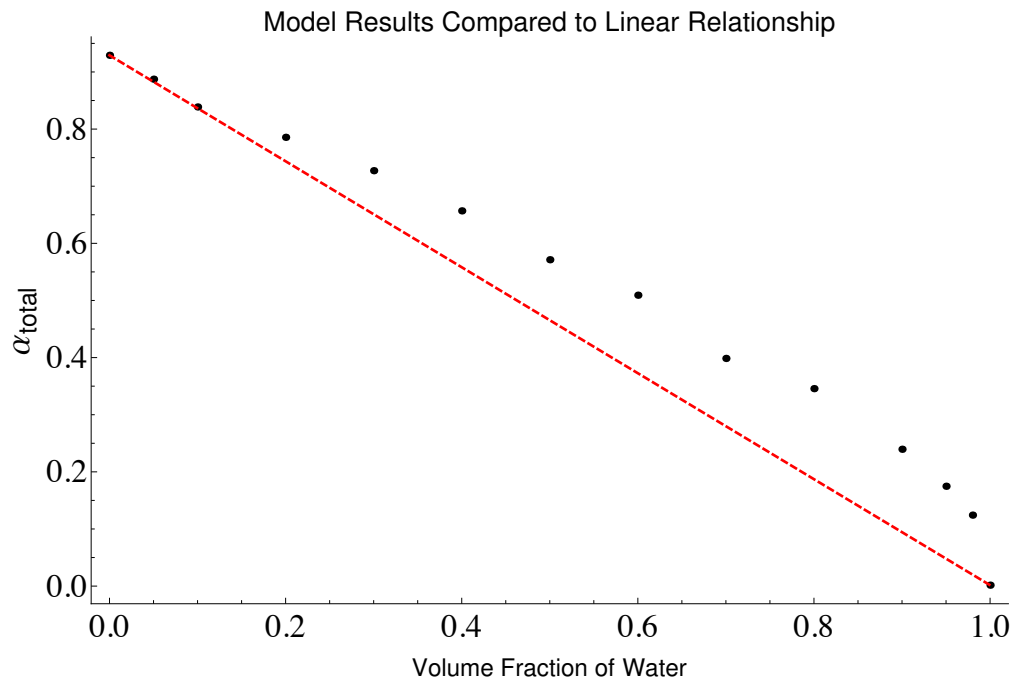


**Figure 3.3** Bulk attenuation coefficient  $\alpha$  as a function of volume fraction of water in a mixed model of water and blood. Error bars from Poisson statistics are smaller than most data symbols. The coefficient of determination,  $R^2$ , is 0.889 and represents the value of a linear relationship between  $\alpha$  and the volume fraction of water (red, dashed line) if one existed.

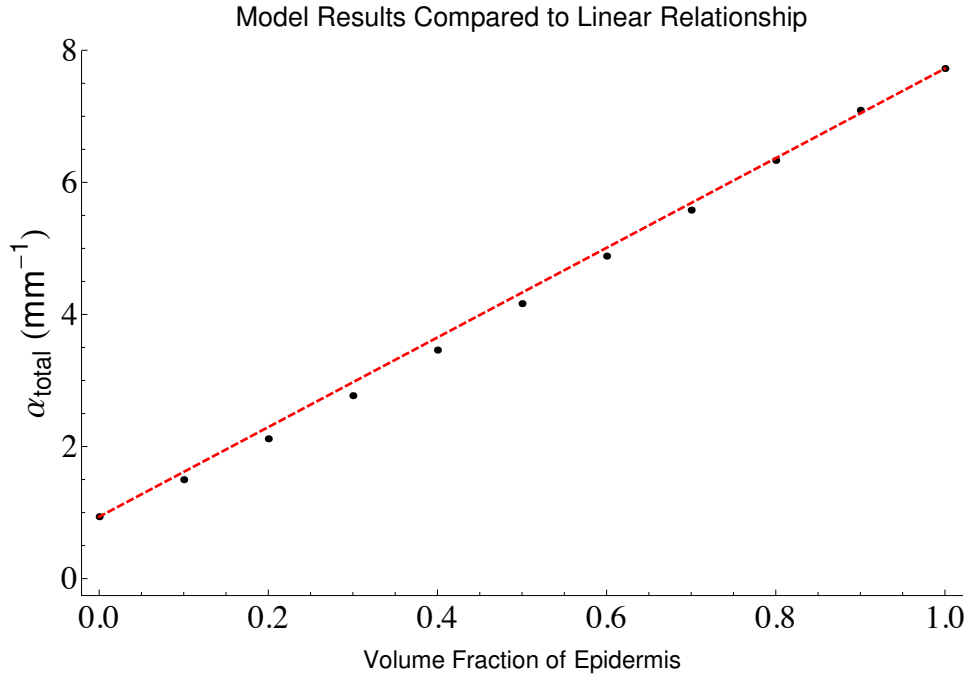


**Figure 3.4** Bulk attenuation coefficient  $\alpha$  as a function of volume fraction of epidermis in a mixed model of epidermis and blood. Error bars from Poisson statistics are smaller than most data symbols. Statistical error bars are shown for each point, but are too small to see for most points. The coefficient of determination,  $R^2$ , is 0.997 and represents the value of a linear relationship between  $\alpha$  and the volume fraction of blood (red, dashed line) if one existed.

The linear relation for  $\alpha_{total}$  in Beer's law as applied to a pair of slabs in contrast (see Eq. (2.22)) is a consequence of the materials being physically and statistically independent. In the layered model, the materials are separated into distinct sections where the propagation distance between interactions depends primarily on one material the photon packet is in (see Eq. (1.6)). As an approximation, we can say that the probabilities of interaction with the different materials are independent of one another, as seen in the modified form of Beer's law (Eq. (2.22)). However, as soon as the materials are mixed together, the propagation distance between interactions is now dependent on all of the materials within the total interaction volume (Eq. (2.27)). Therefore, the mixed model no longer yields statistical independence between the differing materials, and the linear relationship in  $\alpha_{total}$  no longer holds as it did in the layered model.

In terms of the bowling-ball-ping-pong-ball analogy discussed in section 2.3, a material with the larger  $\mu_t$ , or larger interaction cross-section, would be represented by the bowling ball while the one with the lower  $\mu_t$ , or smaller interaction cross-section, would be represented by the ping-pong ball. If we took a mix of balls that was by count 50% bowling balls and 50% ping-pong balls and then separated them into two volumes, such as in the layered model, we would find that the bowling balls would occupy more volume than the ping-pong balls. Thus,  $\alpha_{total}$  would not prorate as 50%  $\alpha_{bowling}$  and 50%  $\alpha_{ping-pong}$ , but rather have a higher weighting of  $\alpha_{bowling}$  than  $\alpha_{ping-pong}$ . As a result, the  $\alpha$  of the material with the higher  $\mu_t$ , in this case the bowling ball, would dominate the curve for  $\alpha_{total}$ . The model with a mixture of water and blood is comparable to this analogy (see Fig. 3.3).

In another situation, we could have  $\mu_{t,1} > \mu_{t,2}$  while  $\alpha_1 < \alpha_2$ . Since  $\alpha$  of a given material is dependent on the anisotropy factor,  $g$ , and  $\mu_t$  is independent of  $g$ , a situation like this could exist if the anisotropy factor of material 2 is lower than that of material 1 (see Eqs. (1.21)-(1.22)). This scenario can be represented by large, light-weight plastic balls (material 1) and small but heavy shot put balls (material 2). Since the plastic balls are larger, they have a higher interaction cross-section ( $\mu_{t,1} > \mu_{t,2}$ ), meaning it is much more likely for a photon packet to interact with them. On the other hand, since they are light-weight, they do not attenuate the intensity of the photon packet as much as the heavier shot put ball would, which corresponds to a lower attenuation coefficient ( $\alpha_1 < \alpha_2$ ). Since  $\mu_{t,1} > \mu_{t,2}$ ,  $\alpha_1$  will dominate the curve for  $\alpha_{total}$ . The model with a mixture of blood and epidermis is comparable to this analogy (see Fig. 3.4).

The direction in which the curve for  $\alpha_{total}$  bends is determined by comparing  $\mu_t$  of the two materials. Whichever material has the higher  $\mu_t$  will have a greater weighting in the total attenuation coefficient,  $\alpha_{total}$ . Thus, if the material with the greater  $\mu_t$  also has a greater  $\alpha$ , then the curve for  $\alpha_{total}$  will bend above the linear relationship (see Fig. 3.3). If the material with the greater  $\mu_t$  has a smaller  $\alpha$ , then the curve will bend below the linear relationship (see Fig. 3.4). How much the

curve for  $\alpha_{total}$  deviates from the linear relationship depends on how much the values of  $\mu_t$  for the two materials differ. In the case of the water-blood mix,  $\mu_{t,blood} \gg \mu_{t,water}$  (see Table 2.1), thus the curve for  $\alpha_{total}$  bends far from the linear relationship (see Fig. 3.3). On the other hand, in the blood-epidermis mixed model,  $\mu_{t,blood} > \mu_{t,epidermis}$ , but they are of the same order of magnitude (see Table 2.1). As a result, although the curve is more weighted to  $\alpha_{blood}$ , the deviation from the linear relationship is small.

In some situations, such as skin where it is composed of sublayers, the layered approximation for Monte Carlo simulations provides a good approximation [8]. In other cases, however, such as in the case of blood where there is no clear boundary between constituents or they are mixed together in a fluid, the mixed model may be better. The mixed model would be the better choice if the  $\mu_t$  values of the materials differed by an order of magnitude or more; otherwise, a layered model may be sufficient. In dosimetry and photodynamic therapy, if one was to assume a linear proration of the attenuation coefficient, one might underestimate how much of the dose is attenuated when delivering radiation to a patient. As a result, the patient could be overdosed with radiation, which could cause unwanted harm to surrounding healthy tissue. Another application is in the case of pulse-oximetry where one is most interested in the blood. The layered approximation may not be elaborate enough to produce accurate results. Pulse-oximetry is very sensitive to simple changes, such as lifting limbs [19]. An accurate model of how light propagates and attenuates in human tissue is of great importance when one wants to use light or other forms of radiation to diagnose or treat patients. The homogeneous mixed model can add further detail to the current models and approximations to obtain even greater accuracy than exists today.

A detailed model including mixing constituents and adding more geometric features of the human finger is an important step in properly simulating the light interactions within the finger. Future research will involve incorporating that structure into our model. In turn, we can develop a more accurate device.

# Appendix A

## Instructions for using Mathematica

This section discusses how to use a Mathematica file, also known as a "notebook."

Each notebook is divided up into "cells," which are lines of code that are grouped together. When the cursor is clicked in a specific cell and the execution command is performed (shift+Enter), then all of the lines of code in that cell will be executed. A brown bar will display on the right, highlighting the square bracket surrounding a cell, showing that the computation is still running. When the brown bar disappears, the computation is complete (see Fig. A.1) Output will display in a new cell just below the input cell. Output and input cells are labeled to the left of each cell in small letters, "In" for input and "Out" for output. The numbers next to these labels represent the order in which the input was executed. Matching numbers for an "In" and an "Out" represent a corresponding input and output, respectively. Sometimes, it is wise to suppress output, such as in the case of a long list of output. This can be accomplished by placing a semicolon after each line of code that you wish to suppress.

A computation that is running may be cancelled at any time through one of two options: "Abort Evaluation" or "Quit Kernel", both which are available under the "Evaluation" menu of the main menu bar of the Mathematica program (see Fig. A.2). If one chooses to perform "Quit Kernel," select "Local", then click "Quit" in the window that appears. Quitting the kernel clears all sym-



The screenshot shows the Mathematica interface with a notebook titled "Running...Monte Carlo Simulation of Photon Propogation\_layered.nb \*". The notebook content is as follows:

```

^ Monte Carlo Simulation

  ^ SetDirectory[NotebookDirectory[]];
    Print[NotebookDirectory[]];
    tissue1name = epidermis;
    tissue2name = blood;
     $\mu$ tissue1 = ToExpression[" $\mu$ " <> ToString[tissue1name]];
     $\mu$ tissue2 = ToExpression[" $\mu$ " <> ToString[tissue2name]];
    Get[ToString[ $\mu$ tissue1] <> ".mx"]
    Get[ToString[ $\mu$ tissue2] <> ".mx"]

     $\lambda$  = 810;
    tissue1 = 1.0;
    tissue2 = 1.0 - tissue1

    C:\Users\Nikki\Documents\Research\

+
In[12]:= min = 10 (*  $\mu$ m *);
        max = 5000 (*  $\mu$ m *);
        spacing = 100 (*  $\mu$ m *);

        Monitor[
          Do[
            ClearAll[positionMatrix, depthProfile, bb, t, b, wCount,
              aveNumSteps, w, wExtLevel, wFinal, stepCount, x, y, z,
              noDetectCount, absorbCount];

            positionMatrix = {{x, y, z}};
            depthProfile = {};
  
```

**Figure A.1** An example of Mathematica running

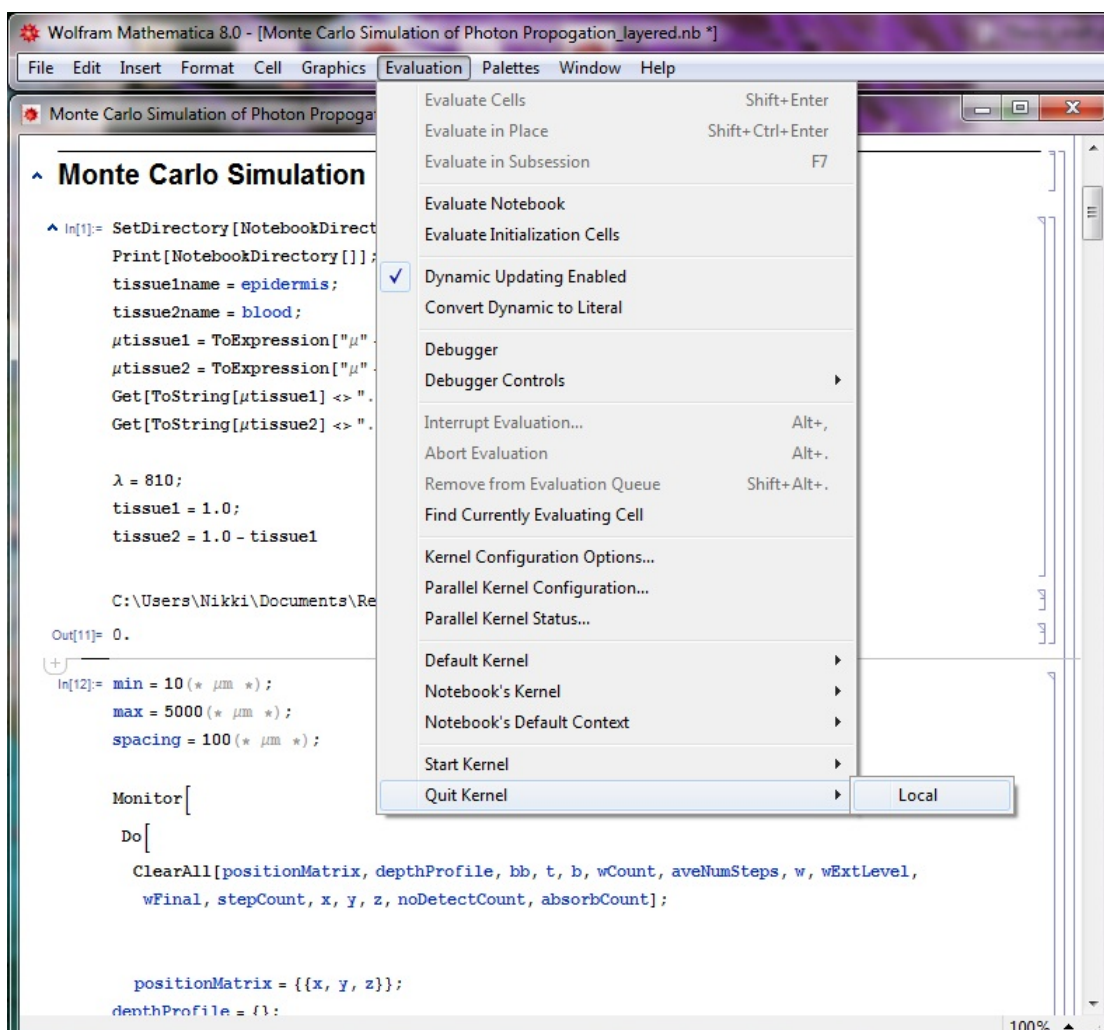


**Figure A.2** Quit the Kernel or abort the evaluation

bolts and values previously defined. Aborting simply stops the evaluation in a certain cell without clearing any values or symbols. When debugging, "Quit Kernel" is very useful.

Commands always start with capital letters. If there are multiple words in a command, each word is capitalized. There is an extensive resource on the format, properties, and examples of all commands available in Mathematica. Simply go to the Documentation Center listed under the "Help" menu (see Fig. A.3). You can search for commands here in the search bar (see Fig. A.4).

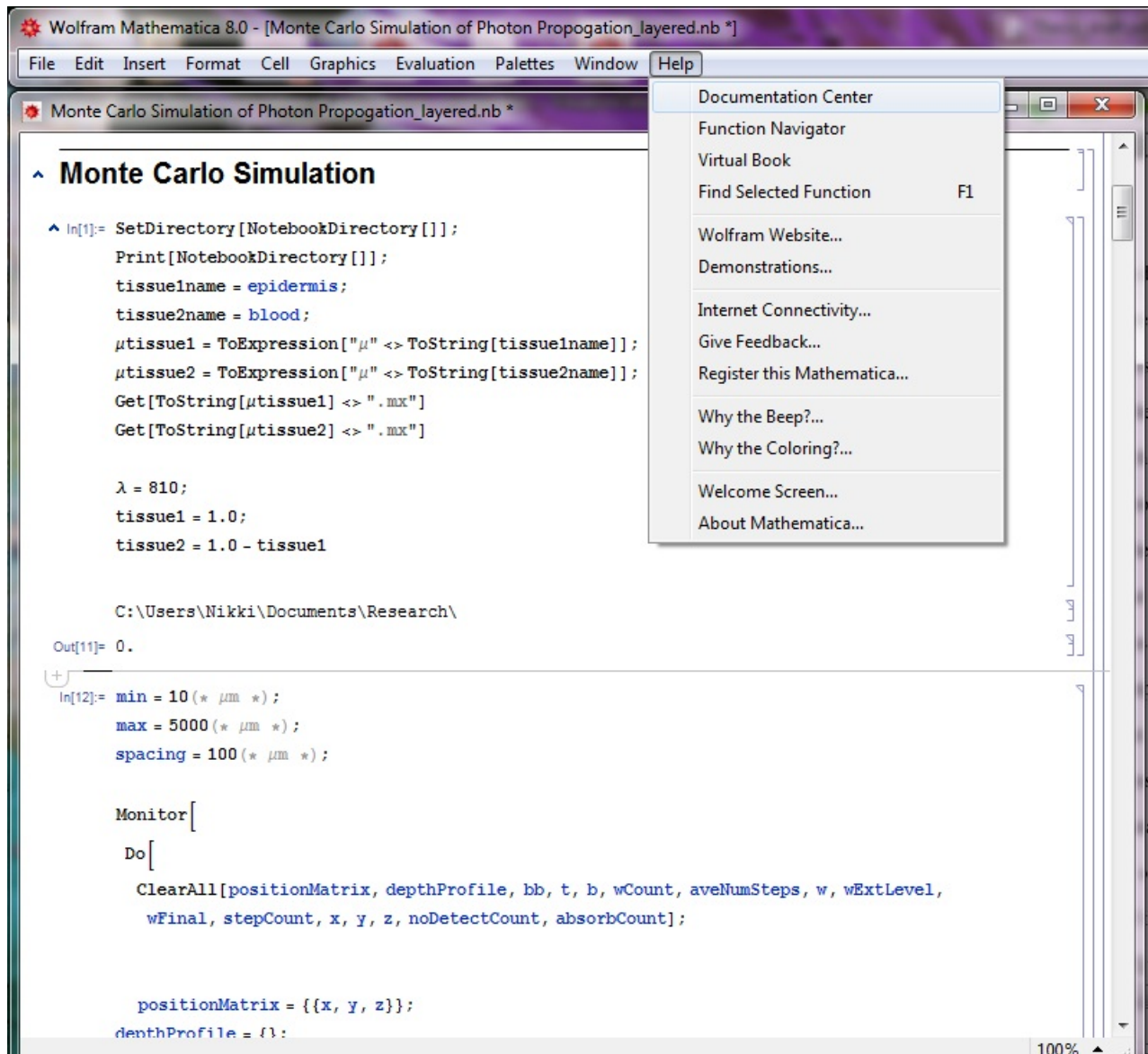


Figure A.3 Locate the Documentation Center

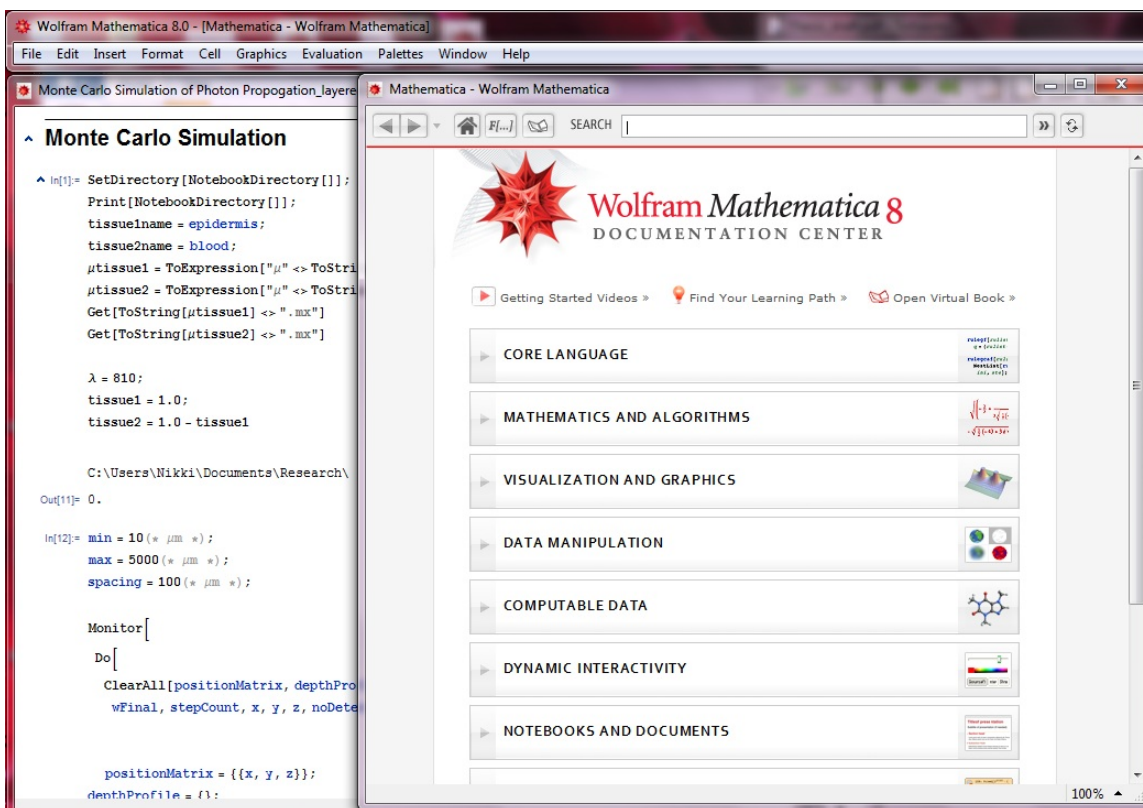


Figure A.4 Documentation Center

## Appendix B

# Instructions for using "Monte Carlo Simulation of Photon Propagation" with the layered model

There are three main notebooks. The Tissue Coefficients one needs to be executed so that the .mx files can be generated on your computer and then be read in through the main simulation notebook. This notebook is used for reading in  $\mu_s$ ,  $\mu_a$ ,  $\mu_t$ ,  $g$  and  $n$  for each type of material. Any time you run the simulation on another computer, you have to regenerate those .mx files as they are unique to each computer. You also have to regenerate those files if you ever make a change to the Tissue Coefficients notebook. Once those files are generated, you can close the notebook.

In the Monte Carlo Simulation notebook, in the first cell, there are two symbols: "tissue1name" and "tissue2name". This is where you define which material is in the top layer (tissue1name) and which is in the lower layer (tissue2name). Even if you want to just work with one material, you need to define both.

Lambda ( $\lambda$ ) is the wavelength, and you need to pick one where there are tissue coefficients for

```

Wolfram Mathematica 8.0 - [Tissue Coefficients_unprimed.nb]
File Edit Insert Format Cell Graphics Evaluation Palettes Window Help

Tissue Coefficients_unprimed.nb

(* (lambda = 517-805 nm) from Tissue Optics, Tuchin, pg. 166; *)
mu_epidermis[lambda_] := With[{lambda = lambda},
  epidermisCount = epidermisCount + 1;
  n = 1.42;
  If[lambda == 577, mu_a = 1.9; mu_s = 48.0; g = 0.787];
  If[lambda == 585, mu_a = 1.9; mu_s = 47.0; g = 0.790];
  If[lambda == 590, mu_a = 1.9; mu_s = 46.0; g = 0.800];
  If[lambda == 595, mu_a = 1.9; mu_s = 46.0; g = 0.800];
  If[lambda == 600, mu_a = 1.9; mu_s = 46.0; g = 0.800];
  If[lambda == 633, mu_a = 3.5; mu_s = 45.0; g = 0.80];
  If[lambda == 810, mu_a = 4.0; mu_s = 42.0; g = 0.85];
  mu_t = mu_a + mu_s;
  mu_sp = mu_s (1 - g);
];
DumpSave["mu_epidermis.mx", mu_epidermis];

(* mu_a and mu_s for dermis:
(lambda = 517-805 nm) from Tissue Optics, Tuchin, pg. 166; *)
mu_dermis[lambda_] := With[{lambda = lambda},
  dermisCount = dermisCount + 1;
  If[lambda == 577, mu_a = 0.22; mu_s = 21.0; g = 0.787];
  If[lambda == 585, mu_a = 0.22; mu_s = 20.5; g = 0.790];
  If[lambda == 590, mu_a = 0.22; mu_s = 20.0; g = 0.800];
  If[lambda == 595, mu_a = 0.22; mu_s = 20.0; g = 0.800];
  If[lambda == 600, mu_a = 0.22; mu_s = 20.0; g = 0.800];
  If[lambda == 633, mu_a = 0.27; mu_s = 18.75; g = 0.80];
  If[lambda == 810, mu_a = 0.23; mu_s = 17.5; g = 0.85];
  mu_t = mu_a + mu_s;
];
DumpSave["mu_dermis.mx", mu_dermis];

```

**Figure B.1** In order to use epidermis and dermis in the same simulation at a specific wavelength, they must both have the coefficients for that specific wavelength.

both materials at that specific wavelength. You can check to see which wavelengths will work by looking in the Tissue Coefficient notebook (see Fig. B.1).

The symbols "tissue1" and "tissue2" define how much of each material you want. So, if you have H2O defined in your "tissue1name", then tissue1=1.0 means that you have 100% volume fraction of H2O and 0% volume fraction of tissue2.

The second cell is the simulation. The symbol "min" is the minimum thickness that the simulation runs through for the whole layered composition, defined in microns. The symbol "max" is

the maximum thickness that the simulation runs through, also in microns. The symbol "spacing" is the interval spacing to the next thickness that the model runs through (in microns as well) (see Fig. B.2). So, if  $\text{min}=1$ ,  $\text{max}=5000$ , and  $\text{spacing}=1$ , the simulation runs through a loop starting at a thickness of  $1\ \mu\text{m}$ , then the next simulation will start over but run through a thickness of  $2\ \mu\text{m}$ , and so on and so on until the simulation resets and runs again with a thickness of  $5000\ \mu\text{m}$ . The Monitor command shows the thickness that the simulation is currently running through at the bottom on the code (see Fig. B.3).

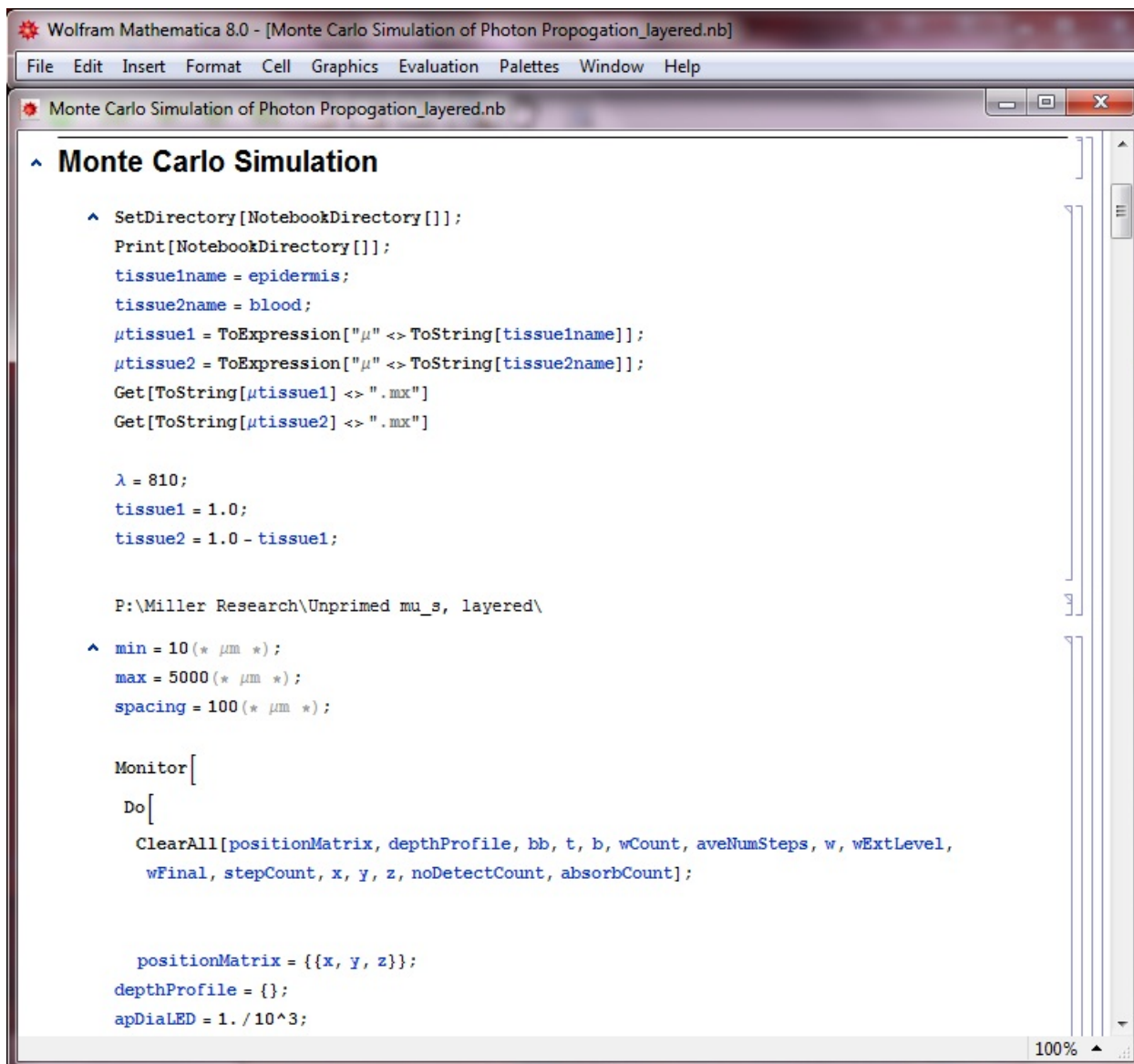
Each full simulation (running through the entire loop, from "min" thickness to "max" thickness) creates four .txt files.

The .txt file with the title "data" gives all the information including the thickness, side-scattering, detected energy, number of photon packets, etc. I rarely use this file, since it is a lot of information. Sometimes, though, it is useful to reference when debugging.

The "energy data...txt" file tells you the intensity of the photon packets that hit the detector for each given thickness. This file can be read into a Mathematica notebook using the ReadList command.

The "Interactions...txt" file keeps track of how many photon packet interactions occur for each material at a given thickness. There is an ordered pair of the form thickness, tissue1 interactions, tissue2 interactions for each thickness the simulation runs through.

The last file is "Track Packets...txt". It keeps tracks of where each photon packet finishes its course given there are only four options for where the packet dies (exit out the top, absorbed in the material, exit out the bottom but do not hit the detector, or hit the detector). This file can also be imported using the command ReadList. The ordered pair has the form thickness, exit out the top, absorbed in the material, exit out the bottom but do not hit the detector, or hit the detector. The total of the second part of that pair should always equal the number of photon packets for each thickness.

The image shows a screenshot of the Wolfram Mathematica 8.0 interface. The title bar reads "Wolfram Mathematica 8.0 - [Monte Carlo Simulation of Photon Propagation\_layered.nb]". The menu bar includes "File", "Edit", "Insert", "Format", "Cell", "Graphics", "Evaluation", "Palettes", "Window", and "Help". The notebook window title is "Monte Carlo Simulation of Photon Propagation\_layered.nb". The main content area is titled "Monte Carlo Simulation" and contains the following code:

```
SetDirectory[NotebookDirectory[]];
Print[NotebookDirectory[]];
tissue1name = epidermis;
tissue2name = blood;
μtissue1 = ToExpression["μ" <> ToString[tissue1name]];
μtissue2 = ToExpression["μ" <> ToString[tissue2name]];
Get[ToString[μtissue1] <> ".mx"]
Get[ToString[μtissue2] <> ".mx"]

λ = 810;
tissue1 = 1.0;
tissue2 = 1.0 - tissue1;

P:\Miller Research\Unprimed mu_s, layered\

min = 10 (* μm *);
max = 5000 (* μm *);
spacing = 100 (* μm *);

Monitor[
  Do[
    ClearAll[positionMatrix, depthProfile, bb, t, b, wCount, aveNumSteps, w, wExtLevel,
      wFinal, stepCount, x, y, z, noDetectCount, absorbCount];

    positionMatrix = {{x, y, z}};
    depthProfile = {};
    apDiaLED = 1. / 10^3;
```

The code defines tissue parameters, sets the directory, and initializes simulation variables. The notebook is displayed at 100% zoom.

**Figure B.2** Starting the Monte Carlo layered model simulation



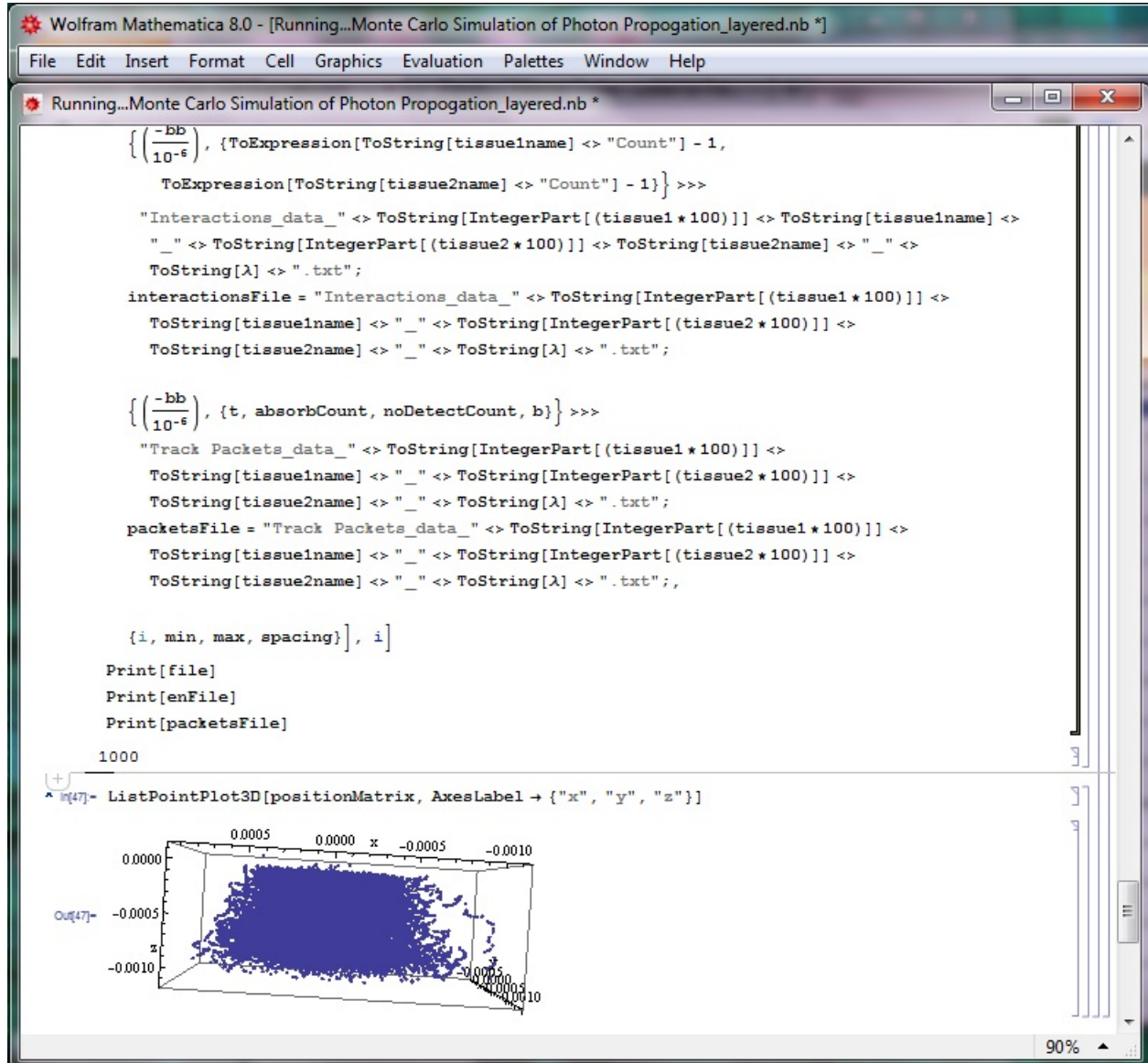


**Figure B.3** While the Monte Carlo simulation is running, a number will display at the end of the main code, such as 1000 in the above figure. This number represents the total thickness (in  $\mu\text{m}$ ) of the model that the simulation is running through at that moment. This number will change from the value that "min" is set to all the way to the value that "max" is set to in increments of "spacing". One can evaluate the next cell down after the simulation is done to show the paths that the photon packets take in the last thickness the simulation ran through.

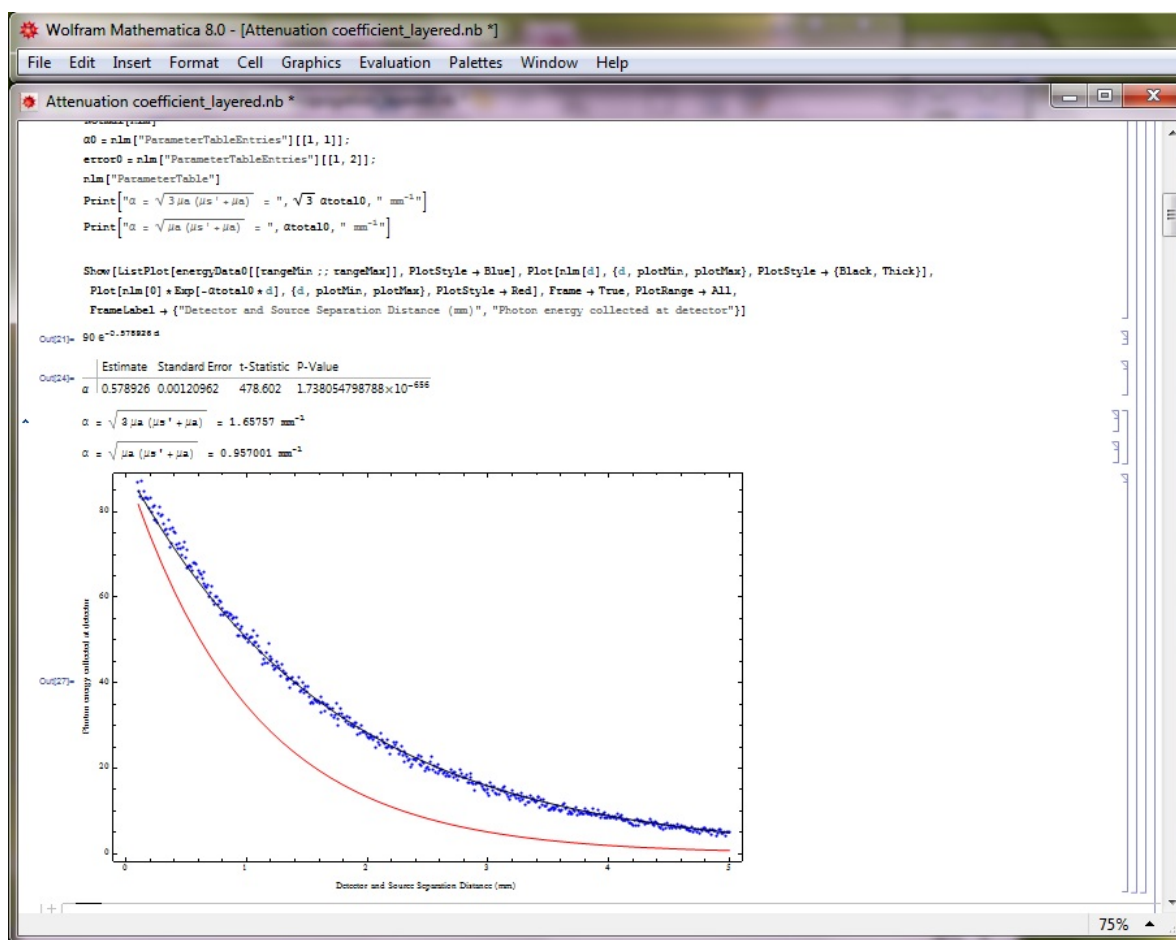


**Figure B.4** Attenuation Coefficient notebook output for curve-fit to data from Monte Carlo simulation

The last notebook, "Attenuation Coefficient," is used for analyzing the "energy data...txt" file and the "Track Packets...txt" file. The first part fits an attenuation coefficient ( $\alpha$ ) for each composition of material. The blue points are the data points from the simulation; the black curve is a fit to the data points from the simulation; the red curve represents the curve with an attenuation coefficient following the  $\alpha = \sqrt{\mu_a(\mu_a' + \mu_s')}$  relationship (see Fig. B.4). The "Track where all photon packets stop" section is for looking at individual compositions (e.g. 100% water or 50/50 water and blood) of the simulation, and seeing where most of the packets end up (exiting out top, being absorbed, etc).

## Appendix C

# Instructions for using "Monte Carlo Simulation of Photon Propagation" with the mixed model

NOTE: See the previous section for screen shots of each of these components—they have the same format in the beginning and end of the notebooks. The only differences are in the middle of the codes, which are not displayed in the screen shots.

There are three main notebooks. The Tissue Coefficients one needs to be executed so that the .mx files can be generated on your computer and then be read in through the main simulation notebook. This notebook is used for reading in  $\mu_s$ ,  $\mu_a$ ,  $\mu_t$ ,  $g$  and  $n$  for each type of material. Any time you run the simulation on another computer, you have to regenerate those .mx files as they are unique to each computer. You also have to regenerate those files if you ever make a change to the Tissue Coefficients notebook. Once those files are generated, you can close the notebook.

In the Monte Carlo Simulation notebook, in the first cell, there are two symbols: "tissue1name" and "tissue2name". This is where you define which materials to simulate with. Even if you want

to just work with one material, you need to define both.

Lambda ( $\lambda$ ) is the wavelength, and you need to pick one where there are tissue coefficients for both materials at that specific wavelength. You can check to see which wavelengths will work by looking in the Tissue Coefficient notebook.

The symbols "tissue1" and "tissue2" define how much of each material you want. So, if you have H2O defined in your "tissue1name", then tissue1=1.0 means that you have 100% volume fraction of H2O and 0% volume fraction of tissue2.

The second cell is the simulation. The symbol "min" is the minimum thickness that the simulation runs through, defined in microns. The symbol "max" is the maximum thickness that the simulation runs through, also in microns. The symbol "spacing" is the interval spacing to the next thickness that the model runs through (in microns as well). So, if min= 1, max= 5000, and spacing= 1, the simulation runs through a loop starting at a thickness of 1  $\mu\text{m}$ , then the next simulation will start over but run through a thickness of 2  $\mu\text{m}$ , and so on and so on until the simulation resets and runs again with a thickness of 5000  $\mu\text{m}$ . The Monitor command shows the thickness that the simulation is currently running through at the bottom on the code.

Each full simulation (running through the entire loop, from "min" thickness to "max" thickness) creates four .txt files.

The txt file with the title "data" gives all the information including the thickness, side-scattering, detected energy, number of photon packets, etc. I rarely use this file, since it is a lot of information. Sometimes, though, it is useful to reference when debugging.

The "energy data...txt" file tells you the intensity of the photon packets that hit the detector for each given thickness. This file can be read into a Mathematica notebook using the ReadList command.

The "Interactions...txt" file keeps track of how many photon packet interactions occur for each material at a given thickness. There is an ordered pair of the form thickness, tissue1 interactions,

tissue2 interactions for each thickness the simulation runs through.

The last file is "Track Packets...txt". It keeps tracks of where each photon packet finishes its course given there are only four options for where the packet dies (exit out the top, absorbed in the material, exit out the bottom but do not hit the detector, or hit the detector). This file can also be imported using the command ReadList. The ordered pair has the form thickness, exit out the top, absorbed in the material, exit out the bottom but do not hit the detector, or hit the detector. The total of the second part of that pair should always equal the number of photon packets for each thickness.

The last notebook, "Attenuation Coefficient," is used for analyzing the "energy data...txt" file and the "Track Packets...txt" file. The first part fits an attenuation coefficient ( $\alpha$ ) for each composition of material. The blue points are the data points from the simulation; the black curve is a fit to the data points from the simulation; the red curve represents the curve with an attenuation coefficient following the  $\alpha = \sqrt{\mu_a(\mu_a + \mu'_s)}$  relationship. The "Track where all photon packets stop" section is for looking at individual compositions (e.g. 100% water or 50/50 water and blood) of the simulation, and seeing where most of the packets end up (exiting out top, being absorbed, etc).

# Bibliography

- [1] T. M. Brand, M. E. Brand, and G. D. Jay, “Enamel nail polish does not interfere with pulse oximetry among normoxic volunteers,” *Journal of Clinical Monitoring Comput.* **17**, 93–96 (2002).
- [2] U. Anaesthesia, “Principles of pulse oximetry,” <http://www.frca.co.uk/article.aspx?articleid=332> (11 Sept 2004).
- [3] J. Severinghaus, “History of Blood Gas Analysis. VII. Pulse Oximetry,” *Journal of Clinical Monitoring* **3**, 135–138 (1987).
- [4] J. Murkin and M. Arango, “Near-infrared spectroscopy as an index of brain and tissue oxygenation,” *British Journal of Anaesthesia* **103**, i3–i13 (2009).
- [5] T. Hamaoka, K. McCully, M. Niwayama, and B. Chance, “The use of muscle near-infrared spectroscopy in sport, health and medical sciences: recent developments,” *Philosophical Transactions of the Royal Society A* **369**, 4591–4604 (2011).
- [6] A. Berger, T. Koo, I. Itzkan, G. Horowitz, and M. Feld, “Multicomponent blood analysis by near-infrared Raman spectroscopy,” *Applied Optics* **38**, 2916–2926 (1999).

- [7] C. for Disease Control and Prevention, “National diabetes fact sheet: national estimates and general information on diabetes and prediabetes in the United States, 2011,” U.S. Department of Health and Human Services, Centers for Disease Control and Prevention (2011).
- [8] L. Wang, S. L. Jacques, and L. Zheng, “MCML—Monte Carlo modeling of light transport in multi-layered tissues,” *Computer Methods and Programs in Biomedicine* **47**, 131–146 (1995).
- [9] Z. Wang, L. Wang, Y. Zhang, and X. Chen, “Monte Carlo simulation of light propagation in human tissue models,” *Bioinformatics and Biomedical Engineering* **3**, 11–13 (2009).
- [10] S. Prahl, M. Keijzer, S. Jacques, and A. Welch, “A Monte Carlo model of light propagation in tissue,” *SPIE Institute Series* **5**, 102–111 (1989).
- [11] V. Tuchin, *Tissue Optics: Light Scattering Methods and Instruments for Medical Diagnosis*, 2nd ed. (Society of Photo-Optical Instrumentation Engineers (SPIE), Bellingham, Washington, 2007), pp. 4–5, 10–21, 145–191.
- [12] L. Carter and E. Cashwell, *Particle-Transport Simulation with the Monte Carlo Method* (USERDA Technical Information Center, Oak Ridge, TN, 1975), pp. 16–17.
- [13] R. Smith and K. Baker, “Optical properties of the clearest natural waters (200–800 nm),” *Applied Optics* **20**, 177–184 (1981).
- [14] D. Huafeng, J. Lu, W. Wooden, P. Kragel, and X. Hu, “Refractive indices of human skin tissues at eight wavelengths and estimated dispersion relations between 300 and 1600 nm,” *Physics in Medicine and Biology* **51**, 1479–1489 (2006).
- [15] E. Hecht and A. Zajac, *Optics*, 3rd ed. (Addison Wesley, 1997).
- [16] D. Sardar and L. Levy, “Optical properties of whole blood,” *Lasers Med Sci* **13**, 106–111 (1998).

- 
- [17] J. Peatross and M. Ware, *Physics of Light and Optics*, 2011c ed. (2011), p. 78.
- [18] D. Baltas, L. Sakelliou, and I. Zamboglou, *The Physics of Modern Brachytherapy for Oncology* (Taylor & Francis Group, LLC, Boca Raton, FL, 2007), p. 25.
- [19] M. Mars and G. P. Hadley, “Failure of pulse oximetry in the assesment of raised limb intra-compartmental pressure,” *Injury* **25**, 379–381 (1994).